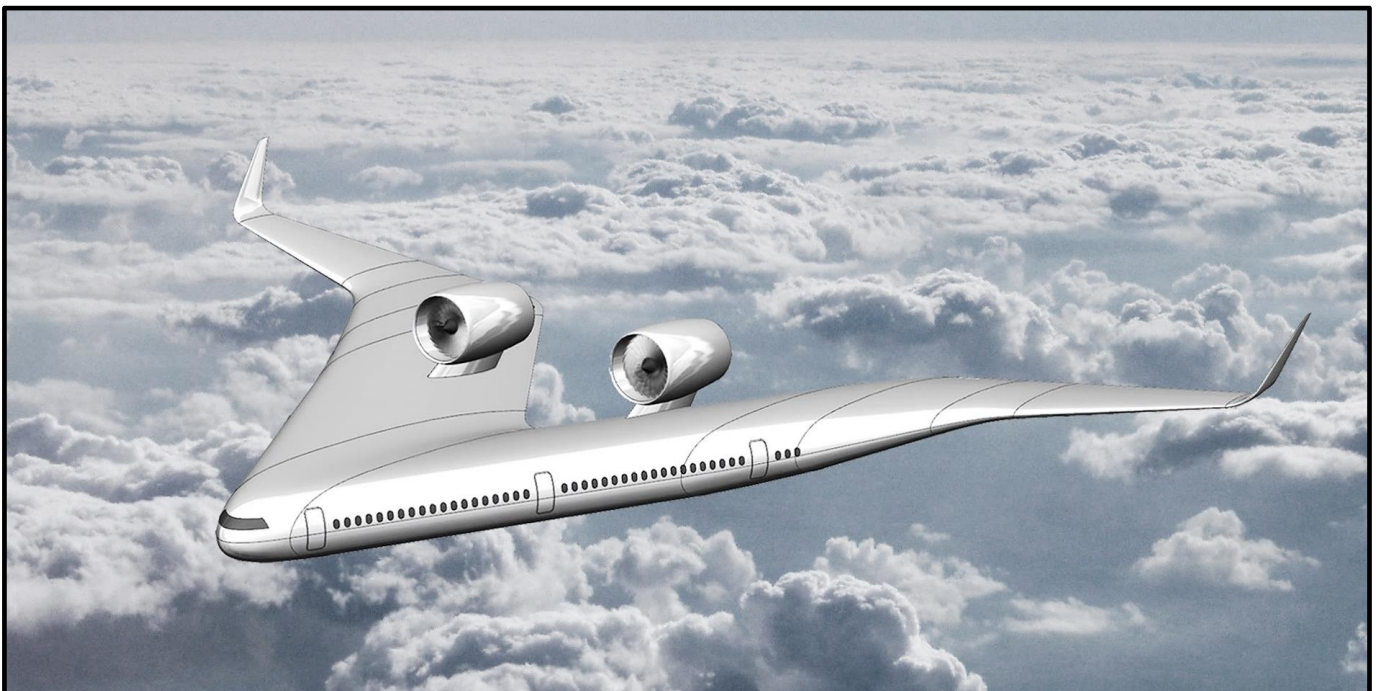


Berlin, 22.03.2015

# **Design of a commercial aircraft for high-subsonic speed as a flying wing configuration**

JUSTUS BENAD



*Deutsche Kurzzusammenfassung:*

## **Entwurf eines Verkehrsflugzeugs für den hohen Unterschall mit Nurflügelkonfiguration**

Ziel der vorliegenden Arbeit ist der Entwurf eines Verkehrsflugzeugs für den hohen Unterschall in Form eines Nurflüglerflugzeugs.

Nach einer Recherche des Stands der Technik von Verkehrsflugzeugen und einer Recherche der geschichtlichen Entwicklung der Nurflüglerflugzeuge sowie deren Flugphysik, werden dazu zunächst grobe Anforderungen an das zu entwerfende Flugzeug aufgestellt. Mit Hilfe dieser Anforderungen wird dann Schritt für Schritt eine neue Konfiguration für den Passagiertransport abgeleitet.

Das Ergebnis ist eine Nurflüglerkonfiguration deren Grundgedanke es ist, zwei im Querschnitt nahezu kreisrunde Druckröhren nach hinten gepfeilt in einer V-Form anzuordnen und diese in dem vorderen Abschnitt eines einzelnen, symmetrischen und an der Vorderkante ebenso stark gepfeilten Flügels zu positionieren. Sich an diesen Mittelflügel anschließende Außenflügel mit geringerem Pfeilungswinkel erhöhen die Spannweite der Konfiguration.

Anschließend wird die nun festgesetzte Konfiguration für 315 Passagiere in einem Zweiklassenlayout entworfen und mit dem A350-900 verglichen. Ziel dabei ist die Beantwortung der Frage, ob die „Flying V“ Konfiguration bei sonst gleichen Hauptauslegungsanforderungen (Nutzlast, Reichweite, Reisegeschwindigkeit, Startstrecke, Passagierkomfort etc.) einen potentiellen wirtschaftlichen Vorteil gegenüber des Referenzflugzeuges aufweisen kann. Um dies zu beantworten werden vor allem die Aerodynamik und die Masse der neuen Konfiguration analysiert und mit dem A350-900 verglichen.

Das Ergebnis ist ein potentieller Vorteil der „Flying-V“ Konfiguration bezüglich der Referenz von 10% (Aerodynamik (L/D)) und 2% (Masse). Weitere Studien werden nötig sein, um diesen Vorteil zu verifizieren und die Machbarkeit der Konfiguration zu zeigen.

Zur Demonstration einiger aerodynamischer Eigenschaften wurde im Rahmen der Arbeit ein funkgesteuertes Modell der „Flying V“ Konfiguration entwickelt. Auf Entwurf, Bau und Test dieses Modells wird in der Arbeit kurz eingegangen.

## Abstract

In this work a new concept for a commercial airplane is derived. The idea is to arrange two pressurized cylindrical sections for the payload swept back in the shape of a V and position them inside the front section of a single wing with the same sweep angle. The concept is designed for 315 passengers in a two class layout and is compared to the reference aircraft, Airbus A350-900. According to the preliminary estimations made in this paper a benefit of 10% in aerodynamics (L/D) and of 2% in mass can be expected of the new configuration over the reference. Further studies will be needed to validate these results and show the feasibility of the concept.

## Acknowledgements

I would like to offer my special thanks to Klaus Bender, my supervisor at Airbus in Hamburg. I am grateful for his trust and for putting me in an innovative environment and giving me a task which led to an idea for a new airplane concept. Klaus patiently introduced me to the many fields of preliminary aircraft design, most of them being completely new to me at the beginning of my work. My thanks also goes to Ingmar Kaulins from the innovation facilitation team at the Future Project Office of Airbus for his great support and the many critical comments on the proposed design.

I would also like to thank the many other colleges from the Future Project Office who have constantly supported me throughout my time at Airbus. The airplane design proposed in this work could have never been created or assessed further without the support and critical comments of Phil Bradshaw, Phil Wright, Fabian Kovacs, Tayfur Kaya, Maximilian Fiedler, Felix Lutsch, Rocco Junk, Georgi Atanasov, Thomas Biwer, Steffen Hammel, Hendrik Friedel, Claus-Peter Gross, Dr. Michael Weismüsler, Karsten Schröder, Yüksel Akyüz, Harry Kwik, Andre Anger and Lars Vollers.

Furthermore, my thanks goes to the great teachers I had before my time at Airbus. My basic understanding of physics, particularly mechanics and fluid dynamics, I owe to Prof. Dr. Popov of the Institute for System Dynamics and Friction Physics of the Technical University of Berlin. He has been a great instructor giving me much of the intuition it took to come up with the design proposed in this work. My thanks also goes to my physics teachers at school Klaus Viebranz and Tom Swayne who introduced me to the world of science and always supported my fascination with aircraft.

I must also express my great appreciation to the people who have encouraged me to further go into the field of preliminary aircraft design and seek the internship at Airbus which has then lead to this paper. I am grateful for the kind advice of Dr. Marin Hepperle concerning the internship. I am also grateful for the support I received from Prof. Dr. Szodruch and his initiative to put me into contact with one of the founding fathers of Airbus, the aircraft designer Dr. Jean Roeder. I couldn't be more thankful for Jean's effort to initiate my internship at Airbus and his continuous support throughout my time in Hamburg as well as the many critical comments on the design proposed in this work. He was excited about the new concept from the moment he saw the very first sketch and this was one great source of encouragement for me throughout the entire design process.

I am very grateful for the help I received from outside of Airbus from Constantin Männel, Andre Holtkämper, Simon Hinsch and Tobias Hinsch with the building and testing of a first radio controlled model of the design proposed in this work.

Finally, I want to thank my friends and family because nothing of this work would have been possible without their support, motivation and enthusiasm.

## Contents

- <i>Abstract &amp; Acknowledgments</i>	ii
- <i>Used symbols</i>	v
- <i>List of figures</i>	vii
- <i>List of tables</i>	x
<b>1. INTRODUCTION</b>	<b>1</b>
<b>2. BRIEF OVERVIEW OF THE STATE OF THE ART</b>	<b>5</b>
<hr/>	
2.1 THE CONVENTIONAL CONFIGURATION	5
2.2 ALTERNATIVES	5
<b>3. FLYING WINGS</b>	<b>7</b>
<hr/>	
3.1 HISTORY	7
3.2 BASIC FLIGHT PHYSICS	10
3.2.1 Longitudinal stability	10
3.2.2 Directional stability	12
<b>4. REQUIREMENTS AND PRELIMINARY ESTIMATIONS</b>	<b>13</b>
<hr/>	
4.1 THE PRESSURIZED VOLUME	13
4.1.1 Efficient use of volume in circular cross section, light circular cross section	14
4.2 THE SPANWISE DISTRIBUTION OF MASS	14
4.3 THE AERODYNAMIC PERFORMANCE	15
4.3.1 A further requirement derived from the requirement of a low wetted area	15
4.3.2 Transonic drag	15
4.4 CG	15
4.5 HIGH LIFT DEVICES	16
4.6 NOISE	16
4.7 MANUFACTURING	16
4.8 OVERALL DESIGN	16
<b>5. THE IDEA GENERATION</b>	<b>17</b>
<hr/>	
5.1 THE TRAIN OF THOUGHT LEADING TOWARDS THE FLYING V	17
5.2 MORE REFINED CONCEPT	22
5.2.1 Change of the cargo configuration	23
5.3 OTHER VARIANTS	24
5.3.1 Other cabin layouts / cross sections	25

<b>6.</b>	<b>PRELIMINARY DESIGN OF THE FLYING V</b>	<b>27</b>
<hr/>		
<b>6.1</b>	<b>STANDARDS &amp; REQUIREMENTS</b>	<b>27</b>
6.1.1	Reference aircraft	27
6.1.2	Cabin requirements	27
6.1.3	Airport constraints	27
<b>6.2</b>	<b>CONCEPTUAL DESIGN</b>	<b>28</b>
6.2.1	Basic geometry	28
6.2.2	Cabin	29
6.2.2.1	Cross section	29
6.2.2.2	Layout	30
6.2.3	Cargo holds	32
6.2.4	Fuel tanks	32
6.2.5	Engine integration	32
6.2.6	Emergency exits	33
<b>6.3</b>	<b>AERODYNAMICS</b>	<b>34</b>
6.3.1	Method	34
6.3.2	Neutral point, longitudinal balance, basic planform selection	35
6.3.3	Performance comparison with the reference aircraft	40
6.3.4	L/D for different CG-positions	41
6.3.5	Some notes on the profile design	42
6.3.5.1	Middle wing	42
6.3.5.2	Transition and outer wings	44
6.3.6	Take-off and landing	44
<b>6.4</b>	<b>MASS EVALUATION</b>	<b>47</b>
6.4.1	Weight breakdown	47
6.4.1.1	Structure	47
6.4.1.2	Power Units, Systems, Furnishings, Operator's items	50
6.4.2	Wing bending and torsion	51
6.4.2.1	Wing bending	51
6.4.2.2	Wing torsion	54
6.4.3	Weight estimation the inner wing structure of the middle and transition wing	55
6.4.3.1	Scaling	55
6.4.3.2	Weight estimation	57
<b>6.5</b>	<b>HANDLING QUALITIES ASSESSMENT</b>	<b>60</b>
6.5.1	CG diagram for loading	60
6.5.2	Directional stability – simulation	61
<b>6.6</b>	<b>RADIO CONTROLLED DEMONSTRATOR MODEL OF THE FLYING V</b>	<b>65</b>
<b>7.</b>	<b>CONCLUSION</b>	<b>69</b>
<hr/>		

## Used symbols

### Upper case letters:

$C_D$	Drag coefficient
$C_{D0}$	Friction drag coefficient
$C_L$	Lift coefficient
$C_M$	Moment coefficient
$C_{M0}$	Moment coefficient for zero lift
$D$	Drag
$E$	Elastic modulus
$F$	An arbitrary force
$I$	Moment of inertia
$L$	Lift
$M$	An arbitrary moment
$Ma$	Mach number
$MAC$	Mean aerodynamic chord
$M_t$	Torsion moment
$MTOW$	Maximum takeoff weight
$OWE$	Operation weight empty
$Q$	Sheer force
$S$	Wing area
$S_c$	Cabin floor area
$S_w$	Wetted area
$T$	Thrust
$V$	Volume
$Y$	Side force (as introduced in Chapter 6.5.2)

### Lower case letters:

$a$	Speed of sound
$b$	Span
$c$	Chord
$cg_{off}$	CG movement to the front from the design point in % of MAC
$d$	Diameter
$c_f$	Friction coefficient
$e$	Oswald factor
$fd$	Upward flap deflection
$f_h$	Fuselage height
$f_{HR}$	Fuselage height ratio
$f_{off}$	Characterizes cabin position, see Chapter 6.2.1
$f_w$	Fuselage width
$g$	Earth's gravitational acceleration
$k$	Wall thickness
$l$	Length
$m$	Mass
$n$	An even number
$p$	Pressure
$q$	Line loading
$\tilde{q}$	Dynamic pressure
$s$	Distance
$sfc$	Specific fuel consumption
$t$	Absolute profile thickness
$v$	Velocity
$y_{\max,pax}$	Maximum distance of passengers from center axis

Upper case Greek letters:

$\Lambda$	Wing aspect ratio
$\Phi$	Bank angle
$\tilde{\Phi}$	Potential of a velocity field
$\psi$	Azimuth angle

Lower case Greek letters:

$\alpha_{cabin,DP}$	Angle of attack of the cabin in the design point
$\beta$	Sideslip angle of the aircraft
$\beta_{cabin}$	Angle of the oblique cabin to the flight direction..
$\beta_{seats}$	Angle of the oblique seats to the flight direction
$\varepsilon$	Local angle of incidence
$\eta$	Dimensionless half span coordinate
$\tilde{\eta}$	Dynamic viscosity
$\vartheta$	Angle of seats inside cabin (see Chapter 6.2.2.2)
$\lambda$	Taper ratio
$\nu$	Dihedral
$\xi$	Static margin
$\rho$	Density
$\sigma$	Stress
$\upsilon$	Intersection angle of circular cabin arcs
$\varphi$	Sweep angle

Additional upper case subscripts:

$BC$	Business class
$EC$	Economy class
$F$	Fuel
$FV$	Flying V
$L$	Lift
$LE$	Leading edge
$MW$	Main wing
$OEI$	One engine inoperative
$OW$	Outer wing
$PL$	Payload
$SP$	Seat pitch
$SR$	Seat rows
$TW$	Transition wing
$WL$	Winglet
25	Measurement is made for the one quarter line of a wing

Additional lower case subscripts:

$cg$	Center of gravity
$n$	Neutral point
$r$	Root
$ref$	Reference aircraft
$t$	Tip
$pax$	Passengers
1g	1g-case
2.5g	2.5g case

## List of figures

Figure 1.1 – The conventional airplane configuration, Boeing 707 from 1960 [2]	1
Figure 1.2 – Growth of air traffic as expected by the aircraft manufacturer Airbus [3]	2
Figure 1.3 – Structure of this work	4
Figure 2.1 – Sketch of the conventional airplane configuration	5
Figure 2.2 – Blended Wing Body concept, EU project NACRE, 2008 [6]	6
Figure 3.1 – An artist’s impression of the Quetzalcoatlus, perhaps one of the first flying wings in the world [8]	7
Figure 3.2 – Planform drawings of various birds by Otto Lilienthal [9]	8
Figure 3.3 – The stork could be characterized as a flying wing having only a small tail which extends the main body to the back almost parallel to the direction of flight, picture from [10]	8
Figure 3.4 – The Éole III, a bat-like flying wing design by Clément Ader which crashed at the first flight, picture from [12]	8
Figure 3.5 – An artist’s impression of Jakob Ellenhammer’s tailless biplane design [14]	8
Figure 3.6 – Igo Etrich successfully built and flew flying wing gliders based on the seed of the Alsomitra Macrocarpa plant in 1907, pictures from [16] and [17]	9
Figure 3.7 – The Dunne D5, a stable flying design with poor aerodynamic efficiency by John Dunne [13]	9
Figure 3.8 – The Stablavion by Rene Arnoux [19]	9
Figure 3.9 – Position of the neutral point for a moderately swept and tapered wing, CG placed in front of it	11
Figure 4.1 – Flat design of the pressurized volume inside a blended wing body [22]	13
Figure 4.2 – Maximum stress in an elliptic pressurized aluminum cylinder at a height of 36000ft with a width of 4.5m, a decreasing height ratio, and a thickness of 6cm	14
Figure 5.1 – Conventional configuration without HTP and high-lift devices, sketch by Klaus Bender	17
Figure 5.2 – Avro Vulcan, picture from [24]	17
Figure 5.3 – Inefficient use of space with a circular pressurized section placed inside of an airfoil	18
Figure 5.4 – Efficient use of space with an elliptical section inside of an airfoil	18
Figure 5.5 – The first two sketches of the proposed configuration	19
Figure 5.6 – When the wetted area is kept the same the cabin area will increase for higher sweep angles	19
Figure 5.7 – Simple swept design with a rather high cabin area to wetted area ratio, first estimation tool by the author	21
Figure 5.8 – Flying V, sketch by the author	22
Figure 5.9 – 3D sketch of the Flying V concept	22
Figure 5.10 – A more refined concept of the Flying V configuration, pictures taken from the second estimation tool “VSP” by Klaus Bender modified by the author	23
Figure 5.11 – First sketch of a possible cross section	24
Figure 5.12 – Configuration as it will be studied in the following chapters of this work	24
Figure 5.13 – The Flying W configuration as an option to further decrease the cg-movement	25
Figure 5.14 – Straight fuselage elements could be added to the design	25
Figure 6.1 – Left: equilibrium of the intersection point of the circular arcs and the floor beam of the cabin cross section, right: intersection angle marked with two lines in a flattened cross section, (estimation tool by the author, the red line marks comfort requirements and the black boxes mark the place for the seats)	29
Figure 6.2 – Variation of the radius of the upper arc of the cross section	30
Figure 6.3 – Selected cross section for the Flying V	30
Figure 6.4 – Cabin concept with oblique seats as it is for instance used on Boeing 777 aircrafts of Delta Airlines, picture from [29]	31
Figure 6.5 – Seats turned relatively to the oblique cabin as a potential measure to increase passenger comfort	31



Figure 6.6 – Engine to engine burst – left: view from the back of the Flying V, right: front view of the CRJ-200	33
Figure 6.7 - Possible evacuation of the Flying V to the back if the front is blocked	33
Figure 6.8 - Exemplary pressure distribution over the Flying V calculated with the Lattice Vortex Method in the tool ODILILA by Klaus Bender	34
Figure 6.9 – Position of the neutral point of the Flying V planform (little dot) with the center of gravity (big checkered dot) 6% MAC in front of it	35
Figure 6.10 – For trimmed flight moments around the longitudinal axis running through the center of gravity must be balanced	36
Figure 6.11 – Untapered wing with different sweep angles optimized for lowest induced drag with a fixed static margin in ODILILA	36
Figure 6.12 – With higher sweep angles the lift distribution can be closer to the shape of an ellipse for wings with same camber and static margin; wing twist of each wing is optimized for lowest induced drag with ODILILA	37
Figure 6.13 – Lift distribution of the Flying V optimized with ODILILA for the geometry set above with a static margin of 6% and uncambered wing sections of the middle wing and wing sections with 2% camber of the transition and outer wings, $C_L=0.25$	38
Figure 6.14 – Planform layout with the geometry set above	38
Figure 6.15 – Upper diagram: twist calculated with ODILILA for the lift distribution shown in Figure 6.13, lower diagram: local $c_l$ values	38
Figure 6.16 – Lifting body of the Flying V viewed from the back, middle wing with constant absolute height (6.10) twists around the horizontal cabin after (6.5) and with the twist determined in this chapter, airplane is trimmed for cruise flight as it is shown in the picture, kinks are blended in the picture	39
Figure 6.17 – $C_M$ over the angle of attack of the cabin floor. Aircraft is longitudinal stable after (3.2) and trimmed for $\alpha=0^\circ$ .	40
Figure 6.18 – $L/D$ over $C_L$ and $L$ , black upper line: Flying V, red lower line: A350-900, marked is the design $C_L$ and the design lift for which the lift distribution of both aircraft has been optimized and for which they are trimmed, curves are then obtained by changing the angle of attack of the aircraft from this point	40
Figure 6.19 – $L/D$ for cruise flight over the center of gravity movement. $cg_{off}$ is given relative to MAC, for example – a positive $cg_{off}=0.1$ means that the center of gravity is 10% MAC to the front of the aircraft from the design position, for negative values it is moved to the back	41
Figure 6.20 – Transonic airfoil and its pressure distribution for $c_f=0.6$ by Whitcomb at $Ma=0.75$ in VGK	43
Figure 6.21 – Symmetrical airfoil with big nose radius and a maximum thickness position at 25% by the author for $c_f=0.2$ at $Ma=0.75$	43
Figure 6.22 – Attempt of an airfoil with a big nose radius and a far up front maximum thickness position without a shock by the author for $c_f=0.2$ at $Ma=0.75$	43
Figure 6.23 – Proposed profile in streamwise direction with elliptical cuts for cabin and cargo section, almost symmetrical profile with an upper surface of a transonic profile and a slight middle loading	44
Figure 6.24 – Cabin and proposed profile	44
Figure 6.25 – Maximum angle of attack of the Flying V at take-off and landing given by the geometry	45
Figure 6.26 – $C_L$ over $\alpha$ , low speed, marked is $C_{L,takeoff}$	45
Figure 6.27 – $L/D$ over $C_L$ , low speed, marked is $C_{L,takeoff}$	45
Figure 6.28 – Cross sections investigated by Airbus, circular arcs added by the author, left picture with $f_{HR}=1$ , right picture with $f_{HR}=0.75$	48
Figure 6.29 – Weight of pressurized structure of the Flying V is estimated by scaling fuselage sections of the A320	48

Figure 6.30 – Distribution of mass and lift over the span for the Flying V at MTOW and cruise flight conditions	51
Figure 6.31 – 1g and 2.5g case: spanwise distribution of mass and lift	52
Figure 6.32 – Line loading of the half span of the Flying V	52
Figure 6.33 – Sheer force distribution	52
Figure 6.34 – Bending moment distribution	53
Figure 6.35 – Section moment of inertia distribution	53
Figure 6.36 – Maximum stress distribution	54
Figure 6.37 – Rough model to estimate the middle wing torsion due to the transition and outer wings of a lower sweep angle	54
Figure 6.38 – Simplified model for the aerodynamic loads	55
Figure 6.39 – Simplified model of the buckling of the skin due to wing bending	56
Figure 6.40 – Simplified model of the compression of the wing ribs due to wing bending	56
Figure 6.41 – Compression and buckling of beams in a framework	56
Figure 6.42 – Additional information on the bending of a pressurized kinked fuselage	59
Figure 6.43 – Center of gravity diagram	60
Figure 6.44 – Rear view of Flying V: half of the center fuel tank is fueled before the transition and outer fuel wing tanks start to be fueled when no fuel pumps are installed	61
Figure 6.45 – Very first quick paper model of the Flying V and more refined paper model of the Flying V, the models fly well and directionally stable with a slight dihedral of the outer wings	61
Figure 6.46 – Flight mechanic model for the movement of the Flying V in the x-y plane, $\Phi=0$ for horizontal flight	61
Figure 6.47 – Flying V with no dihedral of transition and outer wings, disturbance: $\beta=-1^\circ$ , cruise flight	62
Figure 6.48 – Flying V with $6^\circ$ dihedral on transition and outer wings and $16\text{m}^2$ (total) winglets	63
Figure 6.49 – Available height for rear loading ramps to load and unload cargo containers at a dihedral of the transition and outer wings of $6^\circ$	63
Figure 6.50 - Blocks for the wing elements were cut with a hot wire cutter and the profiles were cut out of wood.	65
Figure 6.51 - The profiles were arranged at the calculated position with the calculated twist and the wing shape was made with the hot wire cutter as an even ruled surface.	65
Figure 6.52 – The wings were glued together with styrofoam glue and smoothed with sand paper. The flaps were cut out and the model was covered in a thin layer of glass fiber.	65
Figure 6.53 – Two servos were installed to actuate the flaps. The battery was installed in the front to place the center of gravity to the calculated position.	66
Figure 6.54 – The glider model weighs 770g and has a wing area of $0.43\text{m}^2$ . To achieve the design $C_L=0.25$ a speed of roughly 40km/h is required. After first slower tests with running the model was brought up to 40km/h with a car. The rudders were tested and the model seemed well trimmed for a neutral flap position at this speed and stable.	66
Figure 6.55 – The model was thrown from a little hill out of a height of roughly 3.5m. After a short and fast decent to gain speed after the throw a straight glide path could be taken up on which the Flying V flew roughly 90m. The airplane was easy to control and landed smoothly.	66
Figure 6.56 – With the engines and batteries the weight of the model was increased to 1400g. The required speed for the design $C_L$ is then 50km/h. As engines electro impellers were taken. The batteries were installed in the underbelly.	67
Figure 6.57 – RC model of the Flying V with two birds in the background	67
Figure 6.58 – RC model of the Flying V making a sharp turn	68
Figure 6.59 – RC model of the Flying V on final approach for landing	68

**List of tables**

Table 6.1 – Weight increase of the flat section displayed in Figure 6.28 compared with the circular section	48
Table 6.2 – Pressurized structure of Flying V	49
Table 6.3 – Middle wing / transition wing structure of Flying V, first iteration, not final breakdown	49
Table 6.4 – Outer wing structure of Flying V	50
Table 6.5 – Structure of Flying V, first iteration, not final breakdown	50
Table 6.6 – Operation weight empty of Flying V, first iteration, not final breakdown	50
Table 6.7 – Maximum bending moments of Flying V and reference	53
Table 6.8 – Middle wing / transition wing structure of Flying V, second iteration	58
Table 6.9 – Structure of Flying V, second iteration	58
Table 6.10 – Operation weight empty of Flying V, second iteration	58

# 1. INTRODUCTION

*Il semble que la perfection soit atteinte non quand il n'y a plus rien à ajouter, mais quand il n'y a plus rien à retrancher.<sup>1</sup>*

– Antoine de Saint Exupéry

A flying wing's beauty comes from its simplicity. And as the name says, a flying wing is just a simple wing, nothing more.

As this wing moves at speed through the earth's atmosphere it creates lift counteracting earth's gravity, stays airborne and fulfills its main purpose to fly. In addition to the wing, only a system providing the necessary forward thrust counteracting the wings drag is needed, to keep the wing at speed. Nothing else is necessary to fly<sup>2</sup>.

Now the major purpose of today's aircraft, however, is not only just "to fly" anymore. People or cargo have to be transported *safely* and *efficiently* from one point to the other.

To create an aircraft meeting these demands the designer might just take this simple flying wing and try to store the payload and all other necessary systems inside the wing making use of the volume available in any way.

However, the history of flight has taken a different path. Although the idea of storing all major components of the airplane inside a single wing has long fascinated designers – Hugo Junkers for instance [1, p. 124] (see more in Chapter 3.1) – it has, at least for commercial passenger transport, never come into effect.

Instead, the evolution of commercial passenger aircraft has led to a different design: Rather than connected as a synergistic unit, the parts of the airplane are well separated by their function.



Figure 1.1 – The conventional airplane configuration, Boeing 707 from 1960 [2]

It could be guessed, that one reason why the simple flying wing has not been developed further into an actual passenger aircraft in the cause of the evolution is that the barrier of how to efficiently use the available volume inside such a flying wing could not be overcome.

In this work, this barrier shall be tackled once more. A new idea on how to efficiently use the volume inside a flying wing for passengers will be derived and a configuration proposal will be made with this idea. This configuration will then be compared to a conventional reference aircraft.

---

<sup>1</sup> English translation: "It seems that perfection is attained not when there is nothing more to add, but when there is nothing more to remove."

<sup>2</sup> An accurate definition of a "flying wing" will be given in Chapter 3 of this work. Basic flight mechanics will also be explained in this chapter.

Alongside this rather daring motivation to design a flying wing, drawn merely from intuition and a thesis statement that ways on how to efficiently use the volume inside a wing for passengers may not have been explored enough in the past, there is also a more substantial argument to study flying wing configurations. It shall also be discussed in this introduction before the general outline of the work is described:

According to the aircraft manufacturer Airbus air traffic has roughly doubled every 15 years over the last 45 years and this trend is expected to continue [3].

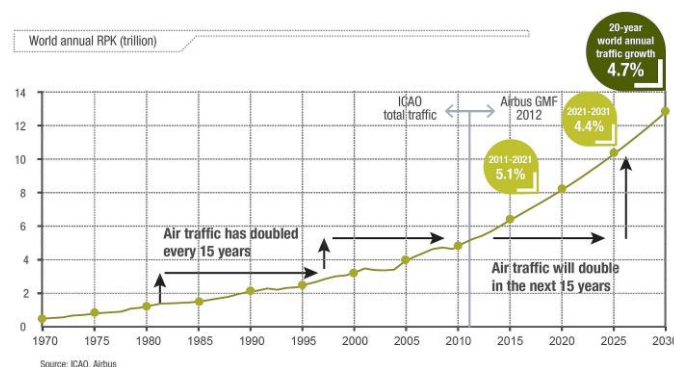


Figure 1.2 – Growth of air traffic as expected by the aircraft manufacturer Airbus [3]

As the airport ground infrastructure is somewhat restricted in its growth capabilities this trend will demand aircraft with larger capacities in the future [3].

In the long run flying wings are likely to be the answer to this trend. When the conventional configuration is scaled up its size is restricted by a proportional growth of the bending stress in the wing root with the scaling factor. This results from the “square cube law” [4]:

When the size is increased with the scaling factor the wing area scales with the second power whereas the volume and thus the mass scales with the third power. This causes the wing loading to scale linearly. Modelling the wing as a simple line loaded cantilever beam the line loading scales with the second power, the root bending moments with the fourth power and thus the stress in the wing root scales linearly with the scaling factor.

This proportional growth of the bending stress in the wing root leads to an over proportional rise of the wing’s mass with the scaling factor. This does not apply for the flying wing configuration because ideally its bending moments are zero due to a spanwise distribution of the payload.

Thus, the flying wing configuration might be of great interest in the future.

Particularly promising seems a flying wing configuration with large capacity. However, also the study of flying wings with conventional capacity remains interesting:

From a theoretical perspective this offers an opportunity to compare a completely new design proposal nicely to an existing reference aircraft. Results may then later be used to assess aircraft of such a new configuration with larger capacities.

From a practical perspective it might indeed be that there is a flying wing design which even with a conventional capacity already exceeds the efficiency of a comparable conventional configuration. This would result in lower operating costs and therefore also be of great interest.

The final result of this work will be a concept of a flying wing configuration with 315 passengers (two class layout) and a comparison of this aircraft with a reference indicating a potential benefit of 10% in aerodynamics and 2% in mass.

The work is structured chronologically following the design and evaluation process of the configuration.

***Introduction (Chapter 1)***

***Short review of the state of the art for commercial passenger transport (Chapter 2)***

The layout of the conventional configuration and well known unconventional configurations will be described *very* roughly. Their advantages and disadvantages will be mentioned.

***General research on flying wing aircraft (Chapter 3)***

The historical development of flying wings will be described. Also, the basic flight physics for flying wings will be discussed.

***Conclusion for the basic requirements for the configuration (Chapter 4)***

With the knowledge obtained in the previous two chapters and some preliminary estimations the basic requirements for the aircraft which shall be designed will be concluded.

***Idea generation (Chapter 5)***

With these basic requirements a configuration idea will be derived.

***Preliminary design of the configuration (Chapter 6)***

The capacity of the aircraft will be set, a reference aircraft will be chosen and more refined requirements for the configuration will be made.

Then the basic geometry will be set.

The aerodynamics and the mass of the flying wing and the reference will be evaluated and compared.

The handling qualities of the flying wing will be assessed and the design and testing of a simple RC model for demonstration will be described.

***Conclusion (Chapter 7)***

With the made comparisons and findings it will be concluded if a potential benefit exists for the configuration. Recommendations for future work will be given.

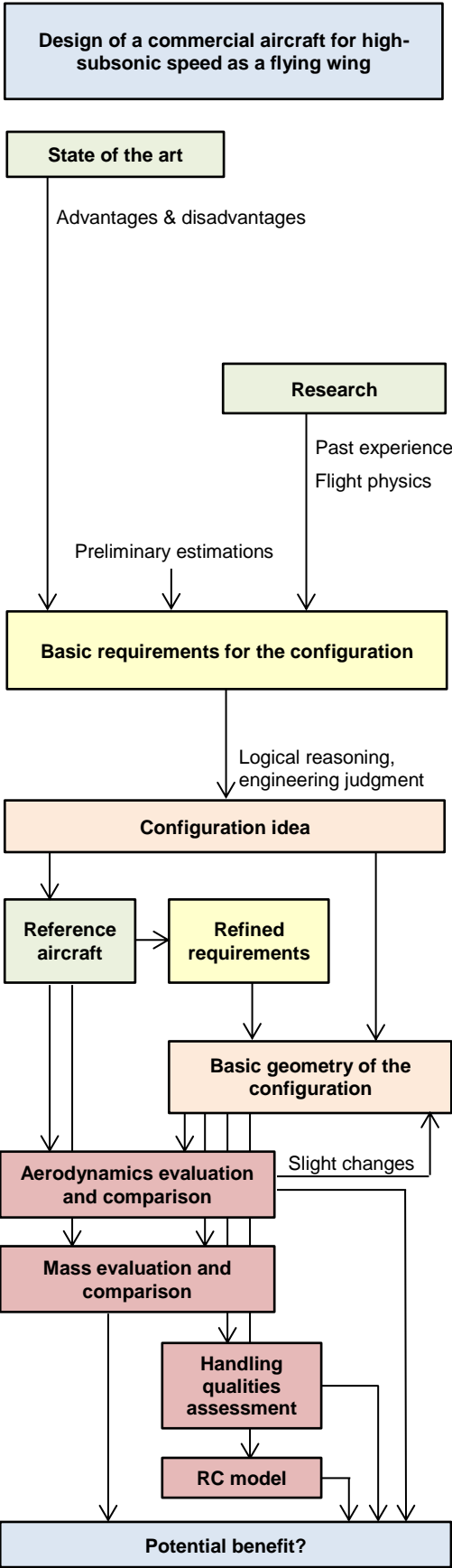


Figure 1.3 – Structure of this work

## 2. BRIEF OVERVIEW OF THE STATE OF THE ART

For an airplane to fly, lift and weight as well as thrust and drag must be balanced. Furthermore, the equilibrium of moments must be fulfilled and the airplane must return to this state of equilibrium after a disturbance.

The general configuration of commercial aircraft has hardly changed over the last 50 years.

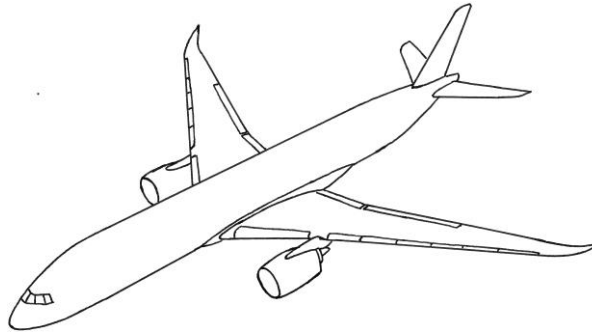


Figure 2.1 – Sketch of the conventional airplane configuration

### 2.1 THE CONVENTIONAL CONFIGURATION

A pipe like fuselage accommodates the payload. Generally, its cross section is circular. This way, internal pressure loads the structure with tension rather than bending and is thus preserved with a minimum of structural mass (see Chapter 4.1).

Wings attached to the fuselage generate the necessary lift, which is proportional to the square of the aircraft's speed and the wing area (see Chapter 4.5).

The aircraft's drag increases with the wetted area and decreases with the wingspan at constant lift (see Chapter 4.3).

In order to minimize the wetted area, the wing area is kept low. This results, however, in the need to modify the shape of the wing at take-off and landing using high lift devices so that enough lift can be generated at such low speeds. High lift devices create large nose down pitching moments and thus, they set the size for the horizontal tailplane, which is commonly located at the fuselage aft section.

As wings are nothing more than line loaded cantilever beams, their weight increases with higher wingspan.

The thrust is provided by engines which are attached to the wing or the fuselage. Mounting the engines at the wing decreases the wing bending moments and therefore the airplane's mass. However, a large vertical tailplane is then needed for the case of an engine failure. When the engines are attached to the fuselage, the vertical tailplane is smaller but the mass of the wings increases.

### 2.2 ALTERNATIVES

Other configurations of commercial aircraft have been proposed and built. One such alternative to the conventional configuration is an airplane without a horizontal tailplane. Planes can fly stable without the horizontal tailplane if the plane can be trimmed and if the center of gravity is located in front of the neutral point (explained in Chapter 3.2). The advantage of this configuration is that the wetted area as well as the mass is decreased because of the missing horizontal tailplane. The disadvantage, however, is that the wetted area is then increased once again because a higher wing area is needed for such a configuration. This is due to the fact that



high lift devices cannot be used without a horizontal tailplane balancing their nose down pitching moment. One more disadvantage of the configuration is that the margin for the center of gravity is very small as the possibilities to trim the airplane efficiently are limited (explained in Chapter 4.4). Therefore, the payload variation would be very limited and a short and wide cabin may be needed.

A radically different configuration is the Blended Wing Body. This design aims to distribute weight and lift over the wingspan so that no bending moments are created. In the case of the Blended Wing Body this is achieved with a highly tapered and large wing with enough room and sufficient height to accommodate passengers in the middle of the wing. However, an increase in mass due to the flat and non-circular shape of the pressurized volume tends to level out the decrease in mass due to the span loaded design and the absence of high lift devices [5]. A significant gain in aerodynamic performance cannot be expected either since the wetted surface cannot be decreased significantly with such a design [6]. The lever arm of the control surfaces to the center of gravity is relatively short. Thus, trimming the aircraft has a considerable impact on the lift distribution which then leads to a high induced drag (see more on this in Chapter 5.2). Furthermore, emergency evacuation is problematic with such a configuration because planform and cabin have only few equal boundaries to the outside.



Figure 2.2 – Blended Wing Body concept, EU project NACRE, 2008 [7]

### 3. FLYING WINGS

In the introduction, the flying wing was proposed as a potential candidate for a new and potentially more efficient airplane configuration.

In its purest form a flying wing is exactly what its name implies. However, also slight variations from the simple wing design are possible. For clarification, the term shall be defined more accurately here.

In the scope of this work a flying wing shall be defined as follows:

*A flying object heavier than air with no more than one lifting surface in the direction of flight.*

*This excludes:*

- *Aircraft with a horizontal tailplane*
- *Canard configurations*

*This includes:*

- *Blended wing bodies*
- *Delta wings*
- *Conventional wing fuselage configurations without a horizontal tailplane*

Thus, the alternatives to the conventional configuration which were just described at the end of the last chapter are indeed flying wings, at least in the scope of this work.

This definition shall, however, not tarnish the picture of the “pure flying wing”, as it will be called in this work from now on, so a flying wing with no extra fuselage exposed to the outside. Such a simple design will still be the design goal in the following chapters.

Before basic requirements for the design can be made though, it shall be looked at the history of flying wings and their basic flight physics in order to get a better understanding of such a design.

#### 3.1 HISTORY

The first flying wings were not men-made. Indeed, they were animals which are believed to have soared the skies long before humans set foot on the earth. The Quetzalcoatlus for instance, was a giant reptile which is believed to have flown 70 million years ago [8].



**Figure 3.1 – An artist’s impression of the Quetzalcoatlus, perhaps one of the first flying wings in the world [9]**

Drawings of more recent examples from nature can for instance be found in the book “Der Vogelflug als Grundlage der Fliegekunst”<sup>1</sup> by Otto Lilienthal from 1891 [10].

---

<sup>1</sup> English translation: “The flight of birds as the basic of the art of flying”



Figure 3.2 – Planform drawings of various birds by Otto Lilienthal [10]

These planforms show that many birds do not need a tail as distinct as on conventional airplane configurations. Indeed, if there is a small tail it is most of the time just the continuation of the bird's main body and not an actual separate surface a significant distance away from the main wing. With this in mind, many birds can be characterized as flying wings.



Figure 3.3 – The stork could be characterized as a flying wing having only a small tail which extends the main body to the back almost parallel to the direction of flight, picture from [11]

Based on his observations of birds Otto Lilienthal designed and successfully flew various gliders. However, he was forced to add horizontal and vertical tail planes to his designs for longitudinal and directional stability [12].

In 1890 Clément Ader attempted a flight of a bat-like flying wing design, however the aircraft was uncontrollable and crashed at the first flight [13].



Figure 3.4 – The Éole III, a bat-like flying wing design by Clément Ader which crashed at the first flight, picture from [13]

Some sources claim that the very first successful flight with a flying wing was made by Jakob Ellenhammer from Denmark in 1906. However, the design was not a pure flying wing being designed as a tailless biplane. Also, it was tethered to a pole in the middle of a circular runway while flying. [14]

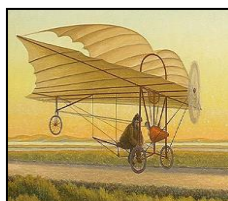
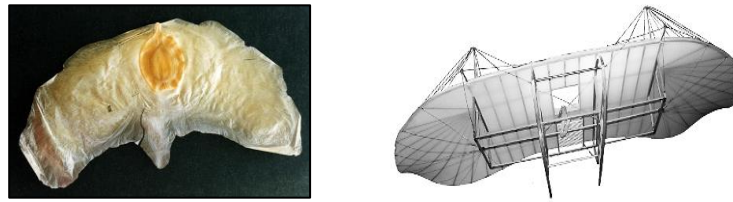


Figure 3.5 – An artist's impression of Jakob Ellenhammer's tailless biplane design [15]

A year later the Austrian Igo Etrich was the first one to make several free, controlled and stable flights with a flying wing. The glider was designed after the seed of the *Alsomitra Macrocarpa* plant which grows in the tropical Asian forests of the Malay Archipelago and the Indonesian islands [16].



**Figure 3.6 – Igo Etrich successfully built and flew flying wing gliders based on the seed of the *Alsomitra Macrocarpa* plant in 1907, pictures from [17] and [18]**

This seed of the *Alsomitra Macrocarpa* is a great example of a pure flying wing which has evolved naturally. It is reported that the large seed with a wingspan of 10cm and a mass of 210g performs elegant glides over long distances of several kilometers. [19]

Other than with birds, one can be sure that the rigid seed is indeed aerodynamically stable<sup>1</sup>. It proves that a stable flight does not necessarily require a second horizontal surface or any vertical surfaces.

After Igo Etrich many more pioneers built flying wings, their main problem being the aerodynamic stability of their designs. Jose Weiss was one of the first to mention the wing twist as a measure for stability which he demonstrated with his flying glider “Olive” in 1909 [14]. John Dunne started to build several different flying wing biplane configurations with swept and twisted wings in 1911 [14].



**Figure 3.7 – The Dunne D5, a stable flying design with poor aerodynamic efficiency by John Dunne [14]**

In 1912 Rene Arnoux built and flew the first flying wing with a reflexed camber line, the Stablavion [20]. This way, another way next to the swept and twisted wing was discovered to design a stable flying wing.



**Figure 3.8 – The Stablavion by Rene Arnoux [20]**

At this time the designers started to realize, that some of their now very stable flying wing configurations had very poor aerodynamic efficiency. However, one was far from assessing the cause of this problem theoretically. The way concepts evolved at this time was just by a continuous try and error selection. [1]

---

<sup>1</sup> These terms will be explained more detailed in Chapter 3.2.

Alexander Lippisch as well as Walter and Reimar Horten refined the geometry of flying wings and improved their aerodynamics to meet the performance of other aircraft of the time in the following years. Lippisch gained much experience with a variety of glider configurations, built the first delta wings, and in 1940 he proved that a conventional design without a horizontal tail can be a successful aircraft: More than 350 airplanes of the Messerschmitt Me 163 were built. The Horten brothers also experimented with a variety of planforms and mainly designed pure flying wing aircraft of a very simple outer shape. [1]

Hugo Junkers should also be mentioned in this context. He never designed a flying wing configuration which was actually built, but it was he who made the first proposal of storing all major parts of the aircraft including the payload inside a wing. His idea was patented in 1910. Until this very day however, it never came into effect for a commercial passenger aircraft designed as a flying wing. His idea was – in part – realized for a conventional configuration though: 1929 the Junkers G38 had its first flight. [1]

Like Hugo Junkers also Jack Northrop was fascinated by the idea of creating an aircraft with all components stored inside the main wing – his focus was, however, on the pure flying wing. He regarded these type of aircraft especially good as bombers and described structural and aerodynamic advantages in a popular speech in 1947. [21]

With today's knowledge, the stability of flying wings is no longer one of the major issues. Leaving away the horizontal tail creates other disadvantages or advantages as briefly described in Chapter 2.2 and as it will be further discussed throughout this work. Especially military airplanes are often designed as flying wings. Two prominent examples from the Cold War are the F7U Cutlass and the Vulcan Bomber. The only commercial passenger aircrafts designed as a flying wing were the Aérospatiale-BAC Concorde and the Tupolev Tu-144. Today, many fighter aircraft are designed as flying wings and the B2 is a very well-known example of a pure flying wing bomber. Recently, also many military drones have been designed as flying wings.

However, the pure flying wing commercial passenger aircraft has not been realized so far.

## 3.2 BASIC FLIGHT PHYSICS

In this sub-chapter the basic flight physics of flying wings will be explained. With a following *preliminary* design study in mind, the model is simplified.

An airplane can here be regarded as a simple rigid body. Such a body has six degrees of freedom. For simple static flight the equilibrium of all forces  $\underline{F}_i$  and all moments  $\underline{M}_i$

$$\sum \underline{F}_i = 0 \text{ and } \sum \underline{M}_i = 0 \quad (3.1)$$

must be fulfilled. For the simplified model this means that thrust and drag as well as lift and weight have to be balanced. Also the moments created by these forces have to be balanced around any arbitrary point. As a further requirement, the airplane has to return to this state of equilibrium after a disturbance, so has to be stable.

### 3.2.1 Longitudinal stability

Intuitively, the longitudinal stability of flying wings is often regarded problematic because of the missing horizontal tail. And as it was just described, the first pioneers indeed struggled with the longitudinal stability. However, the seed of the Alsomitra Macrocarpa proves that a stable flight of a flying wing is possible.

In fact, the requirements which must be fulfilled for longitudinal stability are just the same for a conventional aircraft and a flying wing. It has to be

$$\frac{\partial C_M}{\partial C_L} < 0 \quad (3.2)$$

in a region around the  $C_L$  for which the airplane is trimmed, so for which  $C_M = 0$  [22].<sup>1</sup>

To achieve this, the shape of the airplane has to be in a way that the airplane can be trimmed for the desired lift and the neutral point has to be located behind the center of gravity [22].

The neutral point of an aircraft is the point where the portion of lift depending on the angle of attack of the aircraft acts [22].

For instance, when an airplane flies in trimmed static flight and the angle of attack is increased due to a disturbance the airplane will rise up because of the increased lift. However, the additional aerodynamic force acts behind the center of gravity in the neutral point causing a negative nose down pitching moment decreasing the angle of attack<sup>2</sup> and resulting in a lower lift again which makes the system naturally stable.

It is remarkable that the position of the neutral point only depends on the planform of the aircraft and not on the lift distribution [22].

So when a designer draws the planform of a configuration, flying wing or conventional, this planform sets the neutral point and the rough position of the center of gravity.

Trimming the aircraft then is straight forward for the conventional configuration: The neutral point of a moderately swept wing lies like it is shown in the following figure. With the center of gravity in front of the neutral point most of the airplanes lift will be created behind the center of gravity (if one is to consider in ideal elliptical<sup>3</sup> lift distribution for the wing).

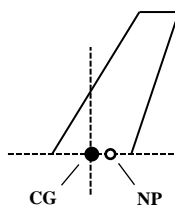


Figure 3.9 – Position of the neutral point for a moderately swept and tapered wing, CG placed in front of it

This causes nose down pitching moments and the aircraft is not trimmed. In addition to that, the commonly used cambered transonic wing section create their lift even further to the back which results in an even higher nose down pitching moment. With a horizontal tailplane creating down force behind the main wing it is easy to trim the airplane. Also the neutral point is shifted more backwards with a horizontal tailplane.

If this configuration with a horizontal tailplane needs to be re-trimmed for any reason this can be done by changing the angle of incidence or the flap deflection of the horizontal tailplane with only a minor influence on the overall lift distribution of the aircraft because a long lever arm exists from the horizontal tail to the center of gravity requiring only small changes in the aerodynamic forces.

<sup>1</sup> For most aircraft  $C_M$  changes linearly with  $C_A$  so that (3.2) also implies that it must be  $C_{M0} > 0$  for an airplane which can be trimmed.

<sup>2</sup> More accurately the angle of attack is also decreased by the upwards movement of the airplane. This is one cause for damping in the stable system.

<sup>3</sup> The induced drag of an aircraft with a given span is minimal when the lift distribution is elliptical. This was derived and published by Ludwig Prandtl here [34, p. 32]. It can be applied to swept designs due to Munk's theorem stating that the overall induced drag does not depend on the position of the lifting elements in flight direction which can be found in [34, p. 41].

This made it easy for the pioneers of aviation to achieve good results quickly with the conventional configuration [1].

For the flying wing one has to think of a different way to trim the aircraft. In order to trim the moderately swept wing shown in Figure 3.9 there are, as already mentioned in the brief historic overview, two options which can also be combined. Making use of a negative wing twist for instance, one can change the lift distribution so that downforce is created at the wing tips. This counteracts the nose down pitching moment and it was done this way by John Dunne on the D5. The aerodynamic performance was not good though, and this was due to the departure from the elliptical lift distribution which caused the induced drag to rise. It is another option to use wing sections with a reflexed chamber line which create their lift far up front and in some cases also downforce at their rear. Thus, they counteract the nose down pitching moment. The overall lift distribution can still be elliptical.

The right choice of wing twist and reflex was difficult to find for the early pioneers [1].

With today's experience and preliminary calculations it is possible to find the right twist and reflex easily. It is even possible to find planforms for flying wing configurations which have an elliptical lift distribution and are longitudinally stable even without reflexed chamber lines and using only a very moderate twist. Such a planform was developed in the course of this work. It will be explained in more detail in Chapter 6.3.2.

### **3.2.2 Directional stability**

Again, the *Alsomitra Macrocarpa* proves that a directional stable flight is possible – even without any vertical surfaces. The requirements for directional stability are, however, not as easily assessed as the requirements for the longitudinal stability. More detailed studies on this matter will be found close to the end of this work in Chapter 6.5.2.

Generally, a positively swept flying wing with a slight positive dihedral is directionally stable. Vertical surfaces such as winglets or a vertical tailplane behind the center of gravity will increase the directional stability.

## 4. REQUIREMENTS AND PRELIMINARY ESTIMATIONS

In this chapter the main requirements for the flying wing configuration which shall be designed will be derived. Some rough estimations will be made to support these requirements.

In the scope of this work “effeciency” will be quantified by the use of Breguet’s formula. With  $\dot{m} = sfc \cdot D$  and

$D = \frac{1}{L/D} \cdot mg$  it can be derived that the distance a plane can travel with a unit of fuel at a certain time during the cruise flight is

$$\frac{ds}{dm} = \frac{a \cdot Ma \cdot L/D}{sfc \cdot m \cdot g} \quad (4.1)$$

With this equation (4.1) in mind and the need to travel at the same speed and with the same  $sfc$  as conventional configurations the goal can be declared to find an aircraft configuration with **a mass as low as possible and an L/D as high as possible.**

In addition to that, many constraints have to be taken into account when designing the flying wing. At this early stage they shall be set as follows:

1. Pressurized passenger cabin and cargo section available with as much capacity as possible
2. Level of passenger comfort must be as high as in existing configurations
3. Aircraft must be possible to trim, aircraft must be longitudinally stable
4. Fast emergency evacuation must be possible
5. Aircraft must be able to take-off and land at existing airports
6. Aircraft must be compatible with the ground infrastructure of existing airports, gate restrictions depending on the aircraft size must be satisfied

Requirements for the aircraft will now be derived from these constraints and the goal of a low mass and a high L/D. Some of the requirements might be in conflict with each other. It will be the goal of Chapter 5 to find a configuration with few conflicts and not violating the constraints.

### 4.1 THE PRESSURIZED VOLUME

The first point to be addressed shall be the shape of the pressurized volume of the aircraft.

As explained in Chapter 2.1, a pipe like fuselage accommodates the payload of the conventional configuration as a very efficient structural solution to preserve the internal pressure.

A prominent example of an unconventional design of the pressurized volume can be found in concepts for blended wing body type of aircraft.

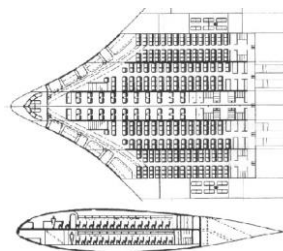


Figure 4.1 – Flat design of the pressurized volume inside a blended wing body [23]



These types of aircraft have a very flat pressurized volume inside the wing to efficiently use the available space for payload. This, however, results in an extremely heavy structure. Recent calculations within the frame of the VELA project have shown that, due to the inconvenient shape of the pressurized volume, the structure will be almost twice as heavy as the structure of a comparable conventional configuration with a circular fuselage cross section. [5]

First principle estimations are enough to illustrate this trend of a rise of mass when moving away from the ideal circular section.

One can for instance get a rough idea on how the stress in a flattened cylinder rises with a simple semi analytical approach for pressurized elliptical pipes with a small wall thickness  $k$  which can be found in [24, p. 152]. (The dimensions in the diagram below are just exemplary and their purpose is to illustrate a trend rather than to give an accurate picture of an actual aircraft.)

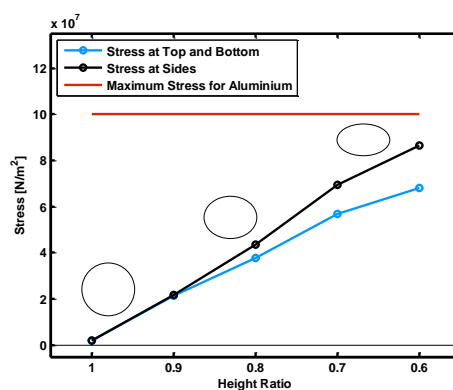


Figure 4.2 – Maximum stress in an elliptic pressurized aluminum cylinder at a height of 36000ft with a width of 4.5m, a decreasing height ratio, and a thickness of 6cm

With these findings and the requirement of a low mass derived from equation (4.1) in mind it follows that the aircraft which shall be designed in this work shall have an **almost circular cross section**.

#### 4.1.1 Efficient use of volume in circular cross section, light circular cross section

Furthermore, it is desirable to efficiently use the volume inside the then circular pressurized cabin. With greater diameters more unused space will arise in the conventional cross sections until the point where a second deck can be used which will then result in a more complicated design. Also, when looking at the linear relation of stress and diameter in the Barlow's formula

$$\sigma = \frac{pd}{2k} \quad (4.2)$$

it follows that the lowest circumferential stress due to internal pressure will be created in a fuselage with a smaller diameter (and then a greater length to offer the same space for the payload).

Accordingly (and looking only at the stress in the pressurized volume created due to internal pressure), it would be desirable to use a rather **long pipe like pressurized volume with a small diameter** to save mass.

## 4.2 THE SPANWISE DISTRIBUTION OF MASS

Another factor of great importance is the spanwise distribution of mass which sets one of the design challenges for the conventional configuration.

The lift distribution over the span of an aircraft should be close to an elliptical shape in order to minimize drag for a given wingspan (further explained in Chapter 6.3). The mass distribution of a conventional aircraft, however, is not elliptical. Instead, most of such a configuration's mass is concentrated in the middle where the fuselage is. This results in high wing bending moments.

As a consequence, the aircraft which shall be designed in this work should ideally be designed with an **almost elliptical mass distribution** so that no bending moments are created.

### 4.3 THE AERODYNAMIC PERFORMANCE

As already mentioned in Chapter 2.1 the aerodynamic performance of aircraft depends mostly on the wetted area and the wingspan. This relation is of great importance throughout the following discussions and shall be derived here. With  $\tilde{q} = \rho v^2 / 2$  and  $mg = \tilde{q} \cdot C_L \cdot S$  for the static cruise flight the relation

$$C_D = C_{D0} + \frac{1}{\pi \Lambda e} \cdot C_L^2 \quad (4.3)$$

can also be written as

$$\begin{aligned} C_D &= C_{D0} + \frac{S}{\pi b^2 e} \cdot \left( \frac{mg}{\tilde{q} S} \right)^2, \\ \tilde{q} S \cdot C_D &= \tilde{q} S \cdot C_{D0} + \frac{S}{\pi b^2 e} \cdot \frac{(mg)^2}{\tilde{q} S}, \\ \text{and then } D &= \tilde{q} S_w c_f + \frac{1}{\pi b^2 e} \cdot \frac{(mg)^2}{\tilde{q}}, \end{aligned} \quad (4.4)$$

which shows that the aircrafts drag and therefore also L/D at a fixed speed and a fixed mass depends only on the wetted area and the span.

Therefore it is desirable for the aircraft which shall be designed in this work to have a **low wetted area** and a **high wing span**.

#### 4.3.1 A further requirement derived from the requirement of a low wetted area

The requirement of a low wetted area leads to the demand to diminish the parts of an aircraft which are exposed to the outside if this is possible without then in return having to increase the size of other parts. A prominent example of such a measure is to install the engines of an aircraft close to the center axis to decrease the size of the vertical tail plane as the yawing moment created by the asymmetric thrust in case of an engine failure is then lower. Therefore it is desirable for the aircraft to have the **engines close to the center axis**.

#### 4.3.2 Transonic drag

For aircraft cruising close to the speed of sound the transonic drag influenced by the wing shape plays a considerable role in the total drag next to the wetted area and the span. Thus, also a **low transonic drag** is required for the aircraft which shall be designed in order to achieve a high performance. This can be achieved with thin streamwise profile sections, sweep and/or low local  $c_f$  values.

### 4.4 CG

The following requirements of this Chapter 4.4 and the Chapter 4.5 are of great importance especially for flying wing type of aircraft.

The center of gravity of an aircraft will move with different loading scenarios and will also move during the consumption of fuel. This requires the aircraft to be trimmed for a certain center of gravity position. Trimming the aircraft adds induced drag though because the lift distribution has to be adjusted to the now changed center of gravity and is thus not optimal anymore (see more in Chapter 6.3.4).

The conventional configuration is trimmed easily by changing the angle of incidence of the whole horizontal tailplane which has a long lever arm to the center of gravity. For a flying wing configuration this second surface does not exist and the aircraft has to be trimmed using flaps on the main and only wing. To minimize the change in the lift distribution necessary for trimming the aircraft it is therefore desirable to design a flying wing aircraft which has either a **short cabin length in flight direction** and **fuel tanks evenly distributed around the center of gravity** (so that the cg movement is low) or has a **long lever arm of the control surfaces to the center of gravity** or some or all of the above.

#### 4.5 HIGH LIFT DEVICES

As previously mentioned in Chapter 2.1 the lift which is generated by a wing is proportional to the square of the aircraft's speed and the wing area:

$$L = \frac{\rho}{2} v^2 \cdot C_L \cdot S . \quad (4.5)$$

As the wing area is kept as low as to minimize the wetted area, the shape of the wing has to be modified at take-off and landing using high lift devices so that enough lift can be generated at such low speeds. However, high lift devices create large nose down pitching moments which have to be trimmed, so they set the size for the horizontal tailplane of the conventional configuration. A flying wing does not have a horizontal tailplane so it is desirable to have **enough wing area to not need high lift devices** at all. Another option would be to use high lift devices which don't make it necessary to trim, for instance as shown in the following picture. The additional lift created with the shown high lift devices is created in front of the center of gravity counteracting the nose down pitching moment.



Flying wing model with pitch neutral flaps, designed and built by Phil Wright

#### 4.6 NOISE

Ideally, the **engines should be shielded from the ground by other parts of the airplane** to reduce noise.

#### 4.7 MANUFACTURING

For cheap manufacturing it is obvious that a simple design is required. Therefore the aircraft which shall be designed in this work shall have **simple and straight lines and few moving parts**.

#### 4.8 OVERALL DESIGN

With the ultimate goal of simplicity of the design in mind the flying wing aircraft shall ideally be designed as a **pure flying wing**, with no extra fuselage exposed to the outside.

Now it is the goal to find a configuration which, ideally, fulfils all these requirements and does not break the constraints mentioned at the beginning of this chapter.

## 5. THE IDEA GENERATION

This chapter will focus on possible solutions of flying wings preferably fulfilling the requirements from the last chapter and it shall be discussed how the barrier which seemed to make it impossible to fulfil some of those requirements in the past with a flying wing configuration could possibly be overcome.

### 5.1 THE TRAIN OF THOUGHT LEADING TOWARDS THE FLYING V

Let us start with the conventional configuration. Wanting to save wetted area the horizontal tailplane should be taken away. **The flying wing which is the outcome of this will not be able to use its high-lift devices because the high nose down pitching moments created by these devices will be difficult to trim without a horizontal tailplane.** The wing area will have to be increased so that the airplane can still take off and land without high-lift devices. The resulting configuration might look like this:

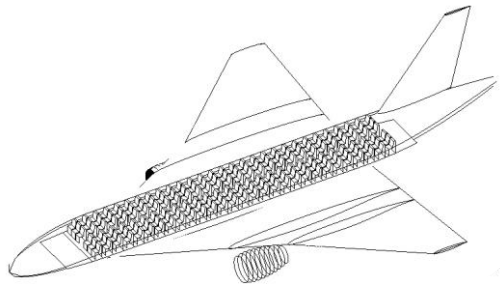


Figure 5.1 – Conventional configuration without HTP and high-lift devices, sketch by Klaus Bender

However, this configuration has some disadvantages:

- Long wing root, cabin difficult to reach for airport vehicles
- Limited possibilities to save wetted area
- Short lever arm of control-surfaces to center of gravity
- Center of gravity movement large for a flying wing

To save wetted area one could think to maybe use the increased wing root to generate more usable volume. For instance, its thickness could be increased to store the engines, as it is the case for the Avro Vulcan. Some wetted area could be saved like this.

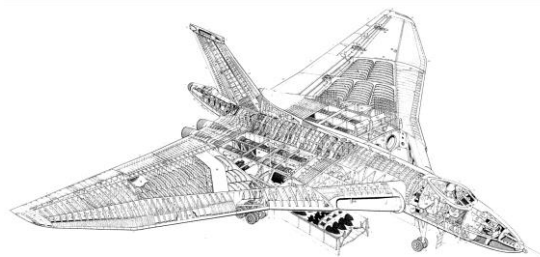


Figure 5.2 – Avro Vulcan, picture from [25]

However, the cg-movement is still high, the wing root is still long and the low lever arm still exists on this configuration. Moreover, structural and maintenance problems may be created with buried engines. Another approach would be to reduce the cabin length with a double decker configuration. But still, not a lot of wetted area could be saved like this, the lever arm

would still be small and a major part of the fuselage would be blocked by the wing-root.

A combination of these two approaches would be to use the space in the greater wing-roots for two more pressurized pipes which could be used as cabin or cargo sections. More thrashed out this design would become a Blended Wing Body aircraft with many circular and connected pipes as a pressurized section. However, such a design would have so few equal lines with the planform that it would be difficult to evacuate. Also, with more and more pressurized pipes one moves further away from the structural concept of a simple fuselage with a circular cross section.

However, let us stress the point of having not one big fuselage but two smaller ones offering the same capacity. According to Chapter 4.1.1 and [26] they will be lighter and more efficient in terms of effective use of space. Side by side they will also decrease the effective length of the cabin in flight direction resulting in a low cg movement. But how to add wings? Adding conventional wings in between and on the outside of the two fuselages would be a connection of many different parts with critical interfaces and few synergies.

So how to arrange the parts in a way which goes together naturally?

Consider arranging the two fuselages in the shape of a V. Just by this simple measure, many of the requirements are fulfilled: The pressurized volume has a circular cross section, it is long and thin (only with a kink), mass is shifted away from the center axis towards a more elliptical mass distribution, and the effective cabin length in flight direction is reduced. Also, both of the fuselages are connected directly to each other which is a far more solid connection already than a thin wing in between two parallel fuselages.

But some sort of wing will be needed to carry the V. It so happens that the design of a flying wing goes perfectly together with the good structural solution of the V. This shall be explained in the following:

If one were to put a circular pressurized section into a conventional airfoil in order to accommodate the payload, a lot of volume would be wasted:



Figure 5.3 – Inefficient use of space with a circular pressurized section placed inside of an airfoil

More desirable would be an elliptical section for the payload:



Figure 5.4 – Efficient use of space with an elliptical section inside of an airfoil

However, then the requirement of a circular and thus light pressurized section would not be fulfilled anymore. *If the circular fuselage is arranged in the shape of a V though, it cuts through the streamwise section in the shape of an ellipse*, just like it is shown in the last picture. So there is indeed a possibility to efficiently use the volume inside a flying wing! And it appears that there might even be a possibility that this solution goes hand in hand with an efficient structural solution for the pressurized volume and many other advantages as described above.

In order for the V shaped fuselage to cut through the wing as it is shown in Figure 5.4, the wing must fully enclose the fuselage and its sweep must follow the shape of the V.

By this measure many more requirements from Chapter 4 are fulfilled. The V shaped design has simple and straight lines. The cabin also has many equal lines with the planform which makes emergency evacuation potentially possible.

Sketches show the configuration idea with a moderate sweep:

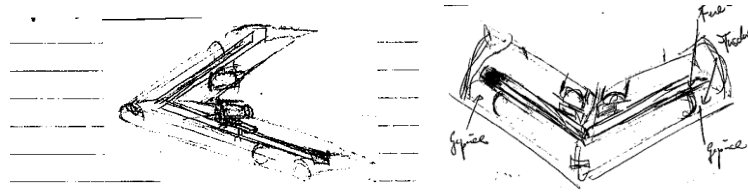


Figure 5.5 – The first two sketches of the proposed configuration

These first drawings were driven mainly by the requirements of a short cabin length in flight direction and a spanwise mass distribution. Also the fuel was placed behind the pressurized cabin with the goal of a low center of gravity movement during its consumption. Cargo was placed inside the pressurized sections at their ends close to the wing tips leaving the room with lower accelerations due to rolling closer to the center axis for passengers. Engines were placed close to the center axis to minimize the moment around the yaw axis in case of an engine failure. They were also placed on top of the aircraft so that their noise will be shielded from the ground.

When the sweep angle is increased the ellipse in Figure 5.4 will lengthen and more volume inside the wing will be taken up by the pressurized section.

This trend can also be expressed in terms of the ratio of the usable cabin floor area  $S_c$  and the wetted area  $S_w$

$$\frac{S_c}{S_w} \sim \frac{1}{\cos \varphi} \quad (5.1)$$

which increases with the sweep angle.



Figure 5.6 – When the wetted area is kept the same the cabin area will increase for higher sweep angles

Also, a higher sweep provides more room for the passengers close to the center axis.

For these two reasons, it was decided to choose a high wing sweep. The upper limit for the wing sweep will be discussed later in this chapter.

Also, the height of the pressurized sections has a direct impact on the wetted area. If  $f_h$  is the height of the fuselage it is

$$f_h \sim S_w \quad (5.2)$$

for a fixed relative profile thickness, wing sweep and span. At a fixed height ratio of the fuselage which is introduced as

$$f_{HR} = \frac{f_h}{f_w} \quad (5.3)$$

where  $f_w$  is the width of the fuselage it follows with (5.2) and (5.3) that

$$S_c \sim S_w \cdot \quad (5.4)$$

So the ratio of the cabin area to the wetted area is not influenced by the width of the cabin if the height ratio is kept constant.

Still, with requirement 4.1.1 in mind it is desirable to have a small cabin cross section to keep the mass low. Therefore, a single aisle cabin shall be chosen as a starting point. As the most effective layout in terms of use of available cabin floor area, a six abreast layout was chosen. This decision will be reviewed in Chapter 5.3.1.

The height ratio  $f_{HR}$  of this cabin will not be fixed at  $f_{HR} = 1$  (as ideally required in Chapter 4.1) as it has an influence on the wetted area

$$f_{HR} \sim S_w \quad (5.5)$$

for a fixed relative profile thickness and cabin width. Reducing the height ratio  $f_{HR}$  will decrease the wetted area for this case, however, as described in Chapter 4.1, it will increase the mass.

Thus, the height ratio will have to be

$$f_{HR} \leq 1 \cdot \quad (5.6)$$

According to Formula (4.4) not only the wetted area has to be minimized for a good aerodynamic performance, but also the wing span has to be maximized.

At this stage, it can be expected that the oblique wing-fuselage-element as it is shown in Figure 5.6 might have a higher cabin area to wetted area ratio  $S_c/S_w$  than conventional airplane configurations<sup>1</sup>.

This is no use however, without a sufficient wing span. With a simple design, a spanwise mass distribution and a low cabin area to wetted area ratio as a goal it would be desirable arrange the elements in the shape of a V (for reasons described above) and not to add anything else to their tips to increase span because then also the wetted area would be increased.

---

<sup>1</sup> For this estimate, consider a conventional long range configuration with a wetted area of roughly  $2100m^2$ , a cabin width of  $6m$  and a cabin length of  $50m$  or a conventional short range configuration with a wetted area of roughly  $880m^2$ , a cabin width of  $4m$  and a cabin length of  $33m$ .  $S_c/S_w$  is then roughly  $0.14 - 0.15$  for these configurations. For the oblique wing fuselage element consider a half-span of  $13m$ , and thus a cabin length of  $31m$  at a sweep of  $65^\circ$ . With a cabin width of  $4m$  and a height ratio of  $0.8$  the chord of the wing has to be  $21m$  at a relative profile thickness of  $15\%$ . This gives a wetted area of  $1300m^2$  for two of these wing elements and a cabin area of  $248m^2$ .  $S_c/S_w$  is then  $0.2$  (roughly  $50\%$  higher than for the conventional configuration).

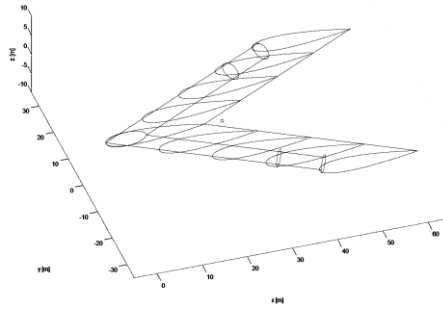


Figure 5.7 – Simple swept design with a rather high cabin area to wetted area ratio, first estimation tool by the author

However, the span of such a basic V-configuration will be limited by the requirement for passenger comfort. If passengers are seated too far away from the center axis they will be subjected to high accelerations due to rolling. In this work the distance which will be allowed for passengers to be away from the center axis will be set<sup>1</sup> to

$$y_{\max, \text{pass}} = 13\text{m} \quad (5.7)$$

which is the distance measured from previous blended wing body concept drawings (VELA [27]).

With a wing span of  $b = 26\text{m}$  the configuration will, however, only have an  $(L/D)_{\max}$  of roughly 14. If wing extensions are used to extend the span up to the gate limit of  $b = 35\text{m}$  of conventional short range aircraft such as the A320 this gives an  $(L/D)_{\max}$  of roughly 15.5.

Estimations for the  $(L/D)_{\max}$  were made with

$$(L/D)_{\max} = \frac{b}{2} \cdot \left( \frac{e\pi}{S_w c_f} \right)^{1/2}, \quad (5.8)$$

which follows from (4.4) and (4.5). For the Oswald factor  $e$  an optimistic first estimate of 0.8 was taken.

The wetted area for such a configuration is higher than for conventional short range configurations, but the ratio of cabin area to wetted area is lower. Indeed, such a cabin would fit roughly 315 passengers at a sweep of 60° in a two class layout which is roughly double the size of a short range aircraft such as the A320.

Therefore, such a short range configuration could still have a possible benefit in terms of fuel consumption as assessed with (4.1) per passenger.

In this work though, such a short range configuration with double the capacity of conventional short range configurations was not studied any further. It was the goal to find a configuration for the same market as an existing aircraft which could then serve as a reference. This was regarded as the simplest way to find out if the idea of using oblique wing-fuselage-segments can be beneficial.

---

<sup>1</sup> It is strongly suggested by the author to also explore configurations with a higher  $y_{\max, \text{pass}}$  and find other ways to decrease the accelerations the passengers are subjected to. If a higher  $y_{\max, \text{pass}}$  would be possible it is believed by the author that the overall efficiency of the aircraft would rise.



However, further work on such a configuration is strongly recommended by the author. Especially the simplicity of the configuration and its compactness make it very attractive for further studies.

Here, a different configuration will be taken. The span of the wing-fuselage-segments arranged in the V shape will be set to  $b = 26m$ . The aerodynamic efficiency as well as the number of passengers rises with a greater span. Therefore, one should go with this upper boundary set with (5.7). As mentioned above, roughly 315 passengers would fit into such an aircraft if the sweep was chosen with  $60^\circ$ . This would be the capacity of a conventional long range aircraft. To compete with such an aircraft's aerodynamic performance though, the wingspan will have to be increased using outer wings attached to the ends of the V shaped wing. This will decrease the ratio of the cabin area to the wetted area of the overall aircraft but will still increase the lift to drag ratio  $(L/D)_{\max} > 20$  as estimations with (5.8) show.

The outer wings shift the neutral point of the configuration further to the back. However Figure 5.8 shows that it will still be possible to place the cabin area and the fuel evenly around the center of gravity which was put 10% MAC in front of the neutral point.

And basically this is the Flying V, as it will be called from this point on. Slight changes to the configuration and the general arrangement will be made throughout the following chapters, but the general configuration of the middle V shaped wing-fuselage sections and the attached outer wings will not change.

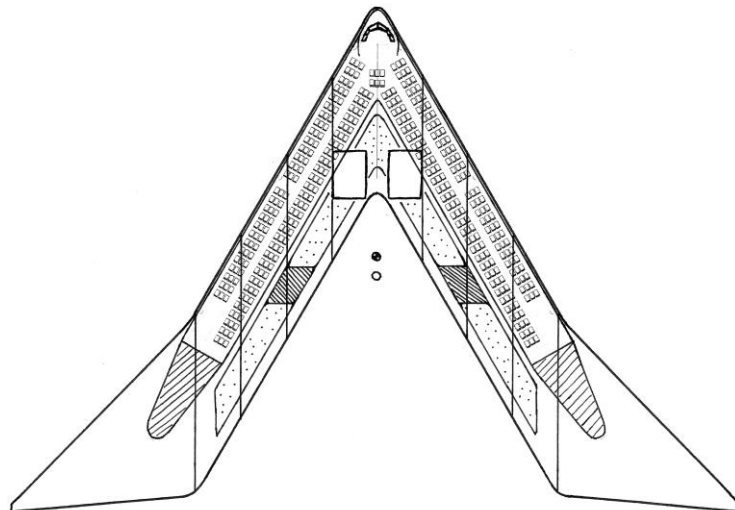


Figure 5.8 – Flying V, sketch by the author

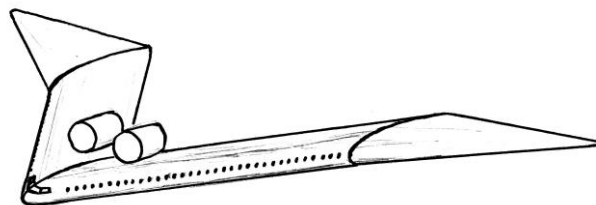
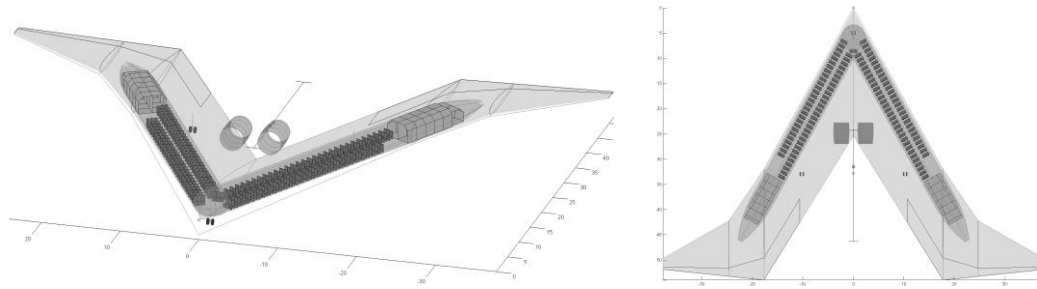


Figure 5.9 – 3D sketch of the Flying V concept

## 5.2 MORE REFINED CONCEPT

To further reduce wetted area transition wings between the middle V shaped wing and the outer wings were inserted. Also the taper ratio of the initially highly tapered outer wings was increased to generate lower local  $c_l$  - values at the tips. (A detailed study of the aerodynamics of the aircraft will be made in Chapter 6.3.)



**Figure 5.10 – A more refined concept of the Flying V configuration, pictures taken from the second estimation tool “VSP” by Klaus Bender modified by the author**

The sweep of the middle wing of the configuration was kept at  $60^\circ$ . According to (5.1) the ratio of the cabin floor area and the wetted area will continue to increase with higher sweep angles. However, it is expected that a higher and higher wing sweep will ultimately result in structural difficulties (as further explained in Chapter 6.4) and handling quality difficulties. As a first engineering judgment the sweep angle will be kept at  $60^\circ$ . This decision will be reviewed in Chapter 6.2.2.2.

The sweep of the outer wings was kept lower than the sweep of the middle wing. This way, more area should be shifted to the front of the aircraft causing the neutral point and thus also the center of gravity of the aircraft to go further up front. This is needed to position the center of gravity in the middle of the cabin area in flight direction so that the cg-movement is decreased. The outer wings will, however have in impact on the structure of the airplane. Torsion in the middle oblique wing sections will be created through the outer wings if they extend the span of the plane at a far lower sweep angle then the sweep of the middle section (see Chapter 6.4.2.2 for an estimation of the wing torsion).

As a further detail, control surfaces for the aircraft were added at the rear of the outer and transition wings and in the back of the V shaped middle wing. One can already see at this stage that the lever arm of the control surfaces to the center of gravity which will roughly have to be located shortly behind the rear kink of the V shaped middle wing will be longer than for planforms where the triangle in between the two oblique shaped wing-fuselage-sections would be filled as it is the case for Blended Wing Body type of aircraft. The neutral point of the latter lies further to the back and so also the center of gravity has to move further back to achieve the same static margin for longitudinal stability. This results in greater flap deflection angles needed to trim the aircraft resulting in a greater change of the lift distribution increasing the induced drag. Also the take-off rotation will be problematic if the center of gravity lies far to the back. This is also due to the small lever arm. On the Flying V though, cutting out the triangle in the back moves neutral point and center of gravity further up front. Thus, requirement 4.4 is also fulfilled with the configuration.

### 5.2.1 Change of the cargo configuration

The cross section of the design<sup>1</sup> shows, that although there is a high wing sweep, it is necessary to use a height ratio of  $f_{HR} < 1$  for the pressurized section in order to efficiently use the space inside the wing.

<sup>1</sup> The cut is made orthogonal to the leading edge of the design

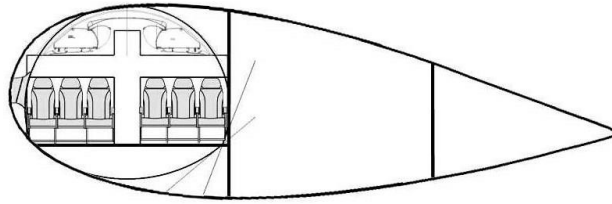


Figure 5.11 – First sketch of a possible cross section

To use the volume inside the middle wing more efficiently it was decided to move the cargo containers from the main pressurized section to a second pressurized section located behind the main section. (Loading and unloading of the cargo will be explained in Chapter 6.2.3).

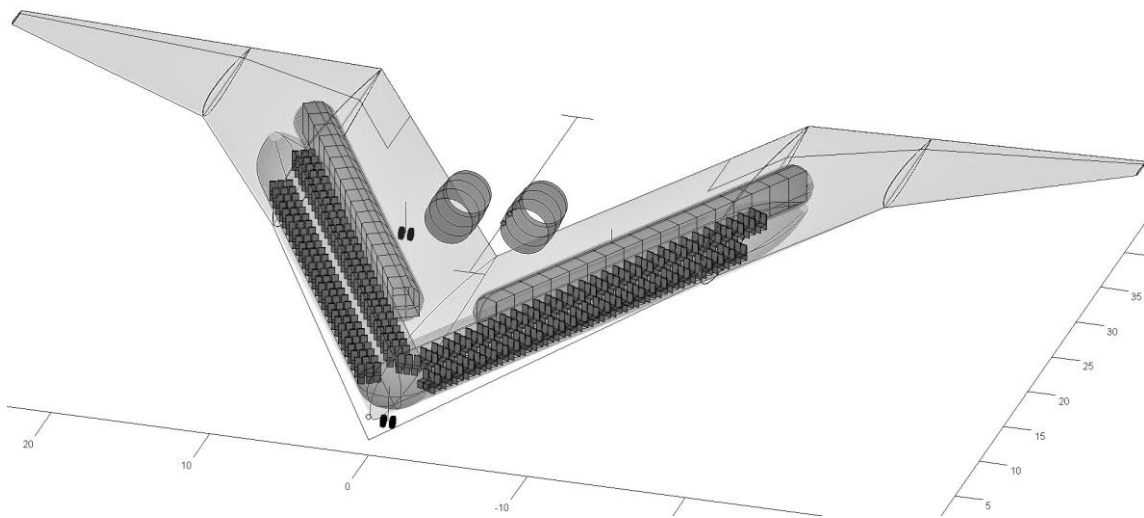
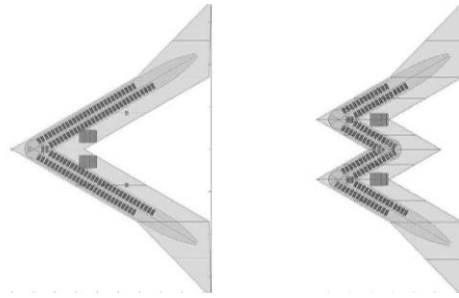


Figure 5.12 – Configuration as it will be studied in the following chapters of this work

Thus, the wetted area of the design can further be decreased. It is this configuration which will be studied further in the following chapters.

### 5.3 OTHER VARIANTS

Before it will be continued with the just described configuration, a few examples of other configurations which would be possible with the idea of oblique wing-fuselage elements of a low cabin floor area to wetted area ratio shall be presented. A promising configuration could be the Flying W configuration. With the same wetted area, the same wingspan, and the same cabin floor area it would have a smaller cabin length in flight direction. Also, the aircraft would be more compact and have a lower footprint. However, the configuration has two more kinks than the Flying V configuration. The kinks in the pressurized structure might increase weight and the kinks in the wing itself might increase drag (as further explained in Chapter 6.3).



**Figure 5.13 – The Flying W configuration as an option to further decrease the cg-movement**

Also, straight fuselage elements could be added to the configuration. The fuselage could be a separation between the two main oblique wing-fuselage elements reducing wave drag or could be used as an extension of the airplane nose also decreasing wave drag. However, such a design would not be as spanloaded as the Flying V design anymore and move away from the pure and simple flying wing. It is, however, an option which should be considered for further work.

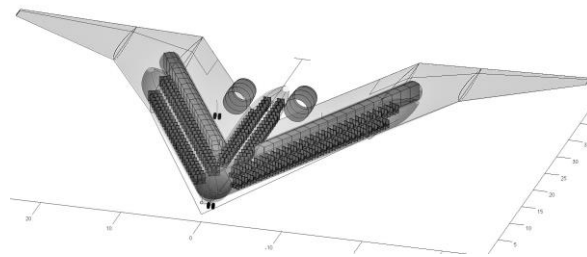


**Figure 5.14 – Straight fuselage elements could be added to the design**

### 5.3.1 Other cabin layouts / cross sections

In the scope of this work it was not possible to further investigate Flying V configurations with different cabin layouts. For reasons described in this chapter, a six abreast layout was chosen. However, this chapter is merely a train of thought leading to an idea and no watertight proof. A five or even four abreast layout might be promising to further investigate. Also, as it was described in 4.1.1, the most efficient use of space inside a fuselage in terms of cabin floor area to wetted area ratio is a large multi decker configuration<sup>1</sup>. This also applies for the oblique wing-fuselage elements the Flying V is made out of:

A double decker layout would offer almost four times as much cabin floor while the wetted area of the middle oblique wing elements would only double.

Such a configuration was not chosen here with the need to evacuate the passengers in mind, with the goal to position as many people as possible close to the leading edge where it might be possible to install windows and with the aim to create a simple design. Also, a lot of unused volume would be created in the not pressurized part of the wing causing the weight to rise.

The first three of these four reasons also caused that a horizontal double bubble configuration was ruled out in this work.

However, these considerations are strongly recommended for future work.

<sup>1</sup> The best use of space in a cylindrical fuselage in terms of usable cabin floor vs. wetted area is theoretically achieved with a multidecker fuselage with an infinitely large diameter because with multiple decks the cabin floor area scales up proportional to the volume.



## 6. PRELIMINARY DESIGN OF THE FLYING V

The Flying V configuration, as it was derived in Chapter 5.2 (Figure 5.12), shall be studied here. This configuration will henceforth be referred to as the “Flying V”.

### 6.1 STANDARDS & REQUIREMENTS

#### 6.1.1 Reference aircraft

The reference aircraft is the Airbus A350-900. It was chosen as it is the state of the art of commercial passenger aircraft with 315 passengers in a two class layout. This roughly matches the capacity of the Flying V.

#### 6.1.2 Cabin requirements

The cabin shape of the Flying V has a direct influence on important aerodynamic drivers such as the wetted area (5.5). Thus, the cabin requirements shall be reviewed here.

Comfort standards of conventional long range configurations such as the reference aircraft must be met by the Flying V configuration.

The standards given by the reference aircraft are as follows:

- Minimum head clearance over the center of the seats closest to the cabin wall:  $1.6m$
- Minimum head clearance in the aisle:  $2.1m$
- Economy class: seat pitch:  $32''$ , seat width:  $20''$ , aisle width:  $18.1''$
- Business class: seat pitch:  $60''$ , seat width:  $29.5''$ , aisle width:  $21.5''$

#### 6.1.3 Airport constraints

The Flying V must be categorized with the same (or a lower) design code / group as the reference aircraft. The codes / groups are set by the FAA and ICAO categorizing airplanes based on wingspan, tail height and main gear wheel span [28]. Upper boundaries for the reference aircraft (Code E / Group V) are:

- Wingspan:  $65m$
- Outer main gear wheel span:  $14m$
- Tail height:  $20.1m$

## 6.2 CONCEPTUAL DESIGN

### 6.2.1 Basic geometry

In this work, the Flying V will be designed so that the angle of attack of the cabin in the design point is

$$\alpha_{cabin,DP} = 0^\circ. \quad (6.1)$$

The aircraft will now be parameterized in this point. The overall global right hand coordinate system will be positioned at the most front tip of the main wing planform. The x-axis is parallel to the center axis pointing to the back of the aircraft, the z-axis points straight up.

The cabin floor is positioned at

$$z_{cabinfloor} = 0. \quad (6.2)$$

The sweep angle of the cabin  $\varphi_{cabin}$  and the leading edge sweep angle of the main wing  $\varphi_{MW,LE}$  are equal:

$$\varphi_{cabin} = \varphi_{MW,LE}. \quad (6.3)$$

The therefore parallel frontlines of main wing and cabin are at an offset  $f_{off}$  measured orthogonal to the leading edge of the main wing. This offset is introduced to ideally position the cabin cross section in the wing profile in horizontal direction. It is

$$f_{off} \geq 0 \quad (6.4)$$

and the greater  $f_{off}$  the easier the cabin fits inside the profile and the harder the installation of doors and windows will be. This will be discussed in further detail in Chapter 6.3.5.

The main wing slightly tapers to the outside. This measure was taken to reduce wetted area. It will be further explained in Chapter 6.3.

The main wing has a linear twist around the trailing edge. The trailing edge itself has a dihedral. Twist and dihedral of the main wing are set so that the wing twists around the cabin and has no dihedral along the center line of the cabin. This is achieved by setting the dihedral of the trailing edge to

$$v_{MW} = \arctan \left( \frac{\left( c_{MW,r} - f_{x,r} \right) \cdot \sin(\varepsilon_{MW,r}) - \left( c_{MW,t} - \left( f_{x,t} - \tan(\varphi_{MW,LE}) \cdot \frac{b_{MW}}{2} \right) \right) \cdot \sin(\varepsilon_{MW,t})}{b_{MW}/2} \right) \quad (6.5)$$

when the twist is given with the local angle of incidence  $\varepsilon_{MW,r}$  at the root of the main wing and  $\varepsilon_{MW,t}$  at the tip.  $c_{MW,r}$  and  $c_{MW,t}$  are the chord lengths at the root and tip and  $f_{x,r}$  and  $f_{x,t}$  are the x-positions of the cabin center line at the root and at the tip of the main wing.

The wing twist will be discussed and calculated in Chapter 6.3. The influence of the resulting middle wing dihedral after (6.5) on the aircrafts handling qualities will be discussed in Chapter 6.5.

The span of the main wing  $b_{MW}$  is set by (5.7), the maximum distance passengers can sit away from the x-axis. For efficient use of volume the pressurized sections are narrowed at their ends making it possible reduce the span of the middle wing which is then continued by transition wings (TW) enclosing the ends of the of the cabin sections. Therefore it is

$$b_{MW} < 26m . \quad (6.6)$$

The transition wings, outer wings (OW) and winglets (WL) extend the span of the aircraft. They are parameterized by span  $b$ , area  $S$ , sweep  $\varphi$ , taper ratio  $\lambda$  (these parameters will be discussed and chosen in Chapter 6.3) and dihedral  $\nu$  (which will be discussed in Chapter 6.5). The overall span of the aircraft is restricted by the gate limit (see Chapter 6.1.3). Therefore,

$$b < 65m . \quad (6.7)$$

## 6.2.2 Cabin

### 6.2.2.1 Cross section

The cross section of the six abreast single aisle cabin shall be designed with the smallest height possible in order to save wetted area, as required by (5.2). The height ratio is restricted by (5.6) but shall be as high as possible to save weight (see Chapter 4.1). Height ratios  $f_{HR} < 1$  can be realized with two circular arcs intersecting at the cabin floor. Cabin pressure causes the arcs to be loaded with tension and compresses the floor.

The free body diagram of the intersection point shows that the compression in the floor column  $B$  increases with higher angles  $\nu$  (Tension forces  $A_1$  and  $A_2$  of the two arcs have to be balanced in vertical direction, thus the geometry necessitates a third force to achieve horizontal equilibrium).

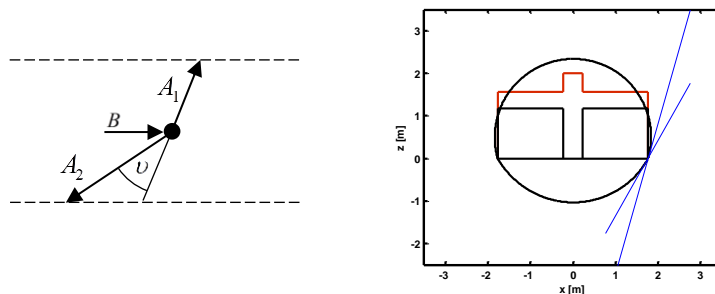


**Figure 6.1 – Left: equilibrium of the intersection point of the circular arcs and the floor beam of the cabin cross section, right: intersection angle marked with two lines in a flattened cross section, (estimation tool by the author, the red line marks comfort requirements and the black boxes mark the place for the seats)**

Buckling of the floor column can be estimated with the second Euler buckling mode [29] and thus occurs when

$$B = \pi^2 \cdot \frac{EI}{l^2} , \quad (6.8)$$

where  $E$  is the modulus of elasticity,  $I$  is the moment of inertia of area and  $l$  is the length of the column.

Therefore, the cross section should have a low angle  $\nu$  and a short floor length  $l$  for a low mass. Also, the radii of the arcs should be small, compare (4.2) for this.

The upper arc can be placed as the following sketch shows meeting the constraints for the cabin comfort (see Chapter 6.1.2).



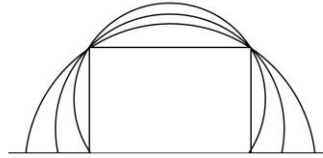


Figure 6.2 – Variation of the radius of the upper arc of the cross section

When lower arcs are attached to the upper arcs shown in Figure 6.2 so that the cabin has always the same overall height,  $\nu$  and  $l$  will get smaller for smaller radii of the upper arc. Therefore, the upper arc has to have the smallest radius allowed by the comfort constraints.

The radius of the lower arc is then an engineering judgment at this point of the design. The higher the lower radius, the lower the cabin height (wetted area goes down at constant relative profile thickness) but the smaller is  $\nu$  (mass goes up). It was selected

$$\nu = 9^\circ . \quad (6.9)$$

The resulting cross section has the following dimensions (inner cabin wall) and is displayed in the following picture.

$$f_h = 3.5m , f_w = 3.7m , f_{HR} = 0.95 . \quad (6.10)$$

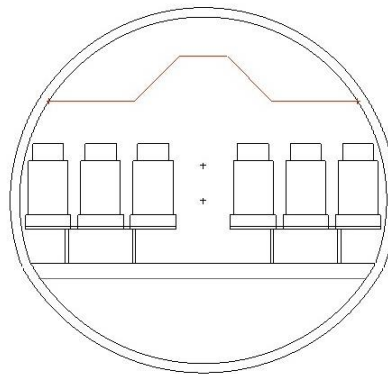


Figure 6.3 – Selected cross section for the Flying V

### 6.2.2.2 Layout

For high sweep angles  $\varphi_{cabin}$  the seats in the pipe like pressurized cabin can be arranged like in a conventional fuselage. The benefit of this is that many similarities will thus exist between the cabin of the Flying V and a conventional configuration.

Passengers are then turned at an angle of

$$\beta_{cabin} = 90^\circ - \varphi_{cabin} \quad (6.11)$$

from the straight flight direction. The high sweep angle of the Flying V causes  $\beta_{cabin}$  to be smaller on the Flying V than the angle  $\beta_{seats}$  the seats are turned relative to the flight direction on some existing commercial aircraft business class cabin layouts (see Figure 6.4).



Figure 6.4 – Cabin concept with oblique seats as it is for instance used on Boeing 777 aircrafts of Delta Airlines, picture from [30]

Turning the seats of the Flying V at an angle  $\vartheta$  relative to the cabin will even decrease  $\beta_{seats}$  of the Flying V:

$$\beta_{seats} = \beta_{cabin} - \vartheta. \quad (6.12)$$

With  $\vartheta = \beta_{cabin}$  a layout with oblique seats as in Figure 6.4 might be possible on the Flying V with the seats facing in flight direction. A potential benefit may be a gain of legroom which is why the design in Figure 6.4 was proposed in the first place [30]. Not as thrashed out as just proposed but only with  $\beta_{seats} = \vartheta = \beta_{cabin} / 2$  a simple sketch is displayed in the following figure.

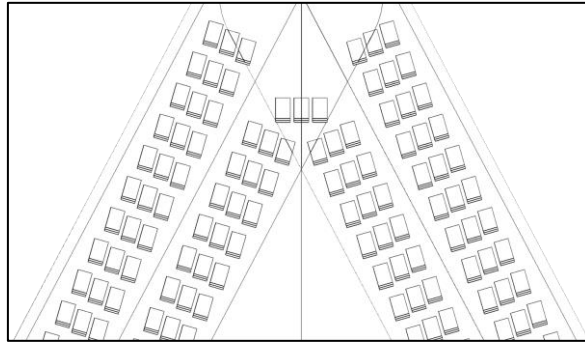


Figure 6.5 – Seats turned relatively to the oblique cabin as a potential measure to increase passenger comfort

A detailed two class cabin layout is not created in this work. In order to compare the capacity of the Flying V with the reference aircraft the length of the nine abreast cabin of the reference aircraft  $f_{l,ref} = 47m$  is divided by the number of seat rows  $n_{SR,ref} = 47$  of the reference aircraft in a one class layout to give an average seat pitch of

$$f_{SP,ref} = 1m \quad (6.13)$$

which is also taken for the Flying V:

$$f_{SP,ref} = f_{SP,FV}. \quad (6.14)$$

The cabin length of the Flying V depends on the sweep angle with

$$f_{l,FV} \sim \frac{1}{\cos(\varphi_{MW})}. \quad (6.15)$$

At a sweep angle of  $\varphi_{cabin} = 63^\circ$  the Flying V has an overall length of the six abreast cabin of roughly  $f_{l,FV} = 70m$ , if it is assumed that the galleys and the rear door can be placed at the outer ends of the cabin at

$y > y_{\max,pax} = 13m$ , as set in (5.7). Both aircraft then have the same capacity of roughly 420 passengers. The sweep angle of the main wing will therefore be set to

$$\varphi_{MW} = 63^\circ \quad (6.16)$$

in order to deal with two aircraft of a comparable size in the following. The choice of the sweep angle will be reviewed in Chapter 6.3 (Aerodynamics) and 6.5 (Handling Qualities).

It is assumed that the capacity of the Flying V and the reference aircraft will be the same in a comparable two class layout also. A two class layout is the standard configuration for the reference and so it shall be for the Flying V. With the chosen geometry and the just made assumption it is then

$$\begin{aligned} n_{pax,BC,FV} &= n_{pax,BC,ref} = 48, \\ n_{pax,EC,FV} &= n_{pax,EC,ref} = 267, \end{aligned} \quad (6.17)$$

and therefore the capacity of the Flying V in a two class layout is henceforth

$$n_{pax,FV} = 315. \quad (6.18)$$

### 6.2.3 Cargo holds

The reference aircraft can store 36 standard LD3 containers in its underbelly. This is a volume of roughly

$$V_{cargo,ref} = 175m^3. \quad (6.19)$$

A cargo volume with a section of  $1.9m \cdot 1.9m$  has to have a length of  $24m$  to offer half the volume of the reference aircraft  $V_{cargo,ref}$ . Thus, two of such cargo section suffice so that

$$V_{cargo,ref} = V_{cargo,FV} \quad (6.20)$$

is achieved.

Placed parallel to and behind the pressurized cabin section they fit into the main wing, as will be shown in Chapter 6.3.5.

Cargo can be loaded and unloaded through rear loading ramps at the ends of the cargo sections. Sufficient height for such a configuration is available due to wing twist and dihedral (see Chapter 6.5.2).

### 6.2.4 Fuel tanks

Fuel tanks are placed in the transition and outer wings and in the center of the middle wing with the goal of achieving a somewhat even distribution of the fuel around the center of gravity in the direction of the longitudinal axis. Additional fuel tanks may be added further to the outside of the middle wing. These might conflict with the movables layout, cargo holds or potential additional exists for emergency evacuation.

### 6.2.5 Engine integration

In this work the engines are placed on top of the aircraft. The engines x-position strongly influences the center of gravity (see Chapter 6.5.1). It will be found, that they will have to be placed behind the main wing rear kink so that the required center of gravity can be achieved.

Thus they cannot be placed directly side by side as it would be ideal for a low yaw moment for an engine failure but have to be placed further away from each other.

For a simple structure, it is desirable to place the engines directly over the main landing gear.

Then, also an engine to engine burst should not be critical for certification, as the following comparison with a certified aircraft shows.

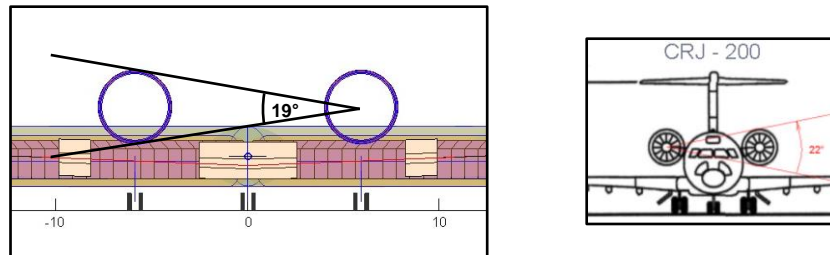


Figure 6.6 – Engine to engine burst – left: view from the back of the Flying V, right: front view of the CRJ-200

Control surfaces and fuel tanks will not be affected at an engine burst due to the swept design. The cabin will be hit at an engine burst, however this is also the case for the conventional configuration.

### 6.2.6 Emergency exits

The worst scenario which could be identified in the scope of this work for the evacuation of the Flying V is a crash in a forest. When all exits to the leading edge would be blocked passengers would have to be evacuated to the rear of the aircraft. The following sketch shows a first idea on how such an evacuation could work. This topic will have to be assessed in more detail in further studies.

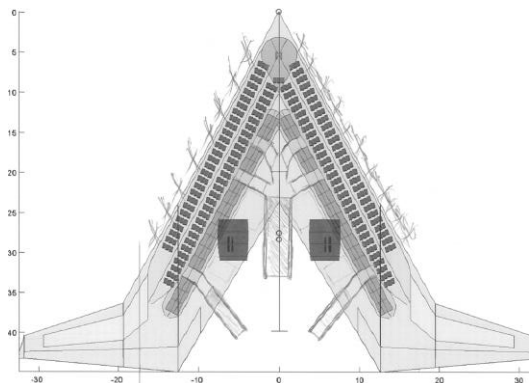


Figure 6.7 - Possible evacuation of the Flying V to the back if the front is blocked

### 6.3 AERODYNAMICS

In this sub chapter the selection of the in Chapter 6.2.1 introduced parameters defining the outer shape of the Flying V will be made and discussed. They shall be chosen so that constraints and requirements set in Chapter 4 and Chapter 6.1, particularly a high  $L/D$  and a sufficient longitudinal stability as described with (3.2) are fulfilled. Results will be compared with the reference aircraft. Anomalies resulting from the unusual design of the Flying V shall be mentioned and discussed.

#### 6.3.1 Method

Both aircraft are evaluated with the same tool and then compared. Thus, a realistic comparison somewhat independent from the used tool shall be achieved.

The tool used is a 3D lattice vortex method called ODILILA which was developed by Klaus Bender in the Future Project Office of Airbus in Hamburg. The purpose of the tool is to optimize the wing (and tailplane) for the best high speed performance and to predict lift and its distribution as well as drag. Also, derivatives for handling quality analyses are calculated.

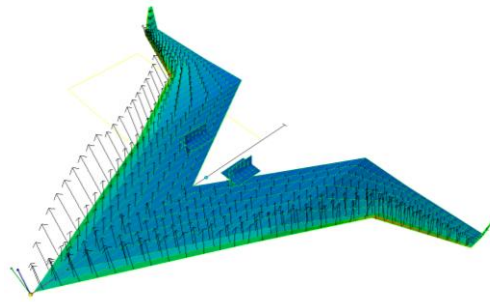


Figure 6.8 - Exemplary pressure distribution over the Flying V calculated with the Lattice Vortex Method in the tool ODILILA by Klaus Bender

The lattice vortex method is an application of the potential flow theory. With the approach

$$\text{rot}(\underline{v}) = 0 \quad (6.21)$$

where  $\underline{v}$  is the vector field of a three dimensional flow it follows directly that a potential  $\tilde{\Phi}$  exists with

$$\underline{v} = \text{grad}(\tilde{\Phi}). \quad (6.22)$$

With the continuity equation for incompressible flow (compare [22])

$$\text{div}(\underline{v}) = 0 \quad (6.23)$$

the Laplace's equation

$$\Delta \tilde{\Phi} = 0 \quad (6.24)$$

follows straight from (6.22).

When (6.24) is inserted into the Navier Stokes equation for incompressible flow [31]

$$\frac{\partial \underline{v}}{\partial t} + \underline{v} \cdot \text{grad}(\underline{v}) = \underline{g} - \frac{1}{\rho} \text{grad}(p) + \frac{\tilde{\eta}}{\rho} \Delta \underline{v} \quad (6.25)$$

one finds together with (6.23) that solutions to (6.24) are also solutions for (6.25).

(6.24) is a homogeneous linear differential equation. Thus, any linear combination of two solutions of (6.24) is also a solution.

Applications of the potential flow theory combine solutions of (6.24) to get an overall solution which is of interest for a particular problem. In Prandtl's classical lifting line theory for instance, vortex filaments are placed in a way to model the potential flow around a wing [22]. For low aspect ratio wings, highly swept wings or plane surfaces of an arbitrary shape this method does not give reasonable results though [22]. The lattice vortex method is a sophistication of the lifting line method to give reasonable results also for those shapes [22].

It is beyond the scope of this work to elaborate on details of the lattice vortex method. The theoretical background is well described in the established literature ([22], [32]).

The lifting surfaces of the method can be arranged to model an aircraft with ODILILA. On the basis of solutions for (6.24) lift distribution, neutral point and induced drag can be computed. Due to (6.21), viscous drag cannot be calculated with the potential flow theory. ODILILA uses an empirical approach for this (the target is a relative comparison of the aerodynamics of Flying V and the reference, so this is acceptable).

ODILILA also does not calculate the wave drag. This will be discussed further in Chapter 6.3.5.

Corrections for compressibility effects are made with the Prandtl-Glauert transformation (compare [33] for an accurate description of the transformation).

### 6.3.2 Neutral point, longitudinal balance, basic planform selection

First, the neutral point of the Flying V planform is calculated with ODILILA. It lies roughly behind the rear kink.

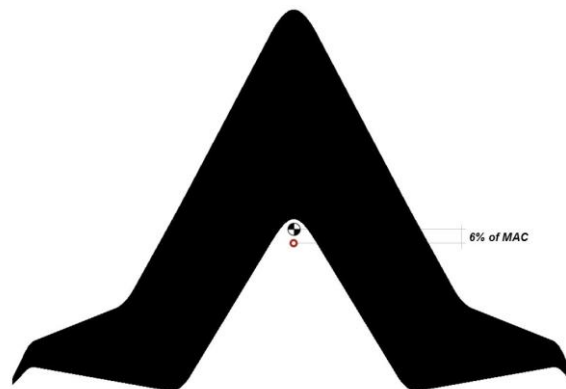
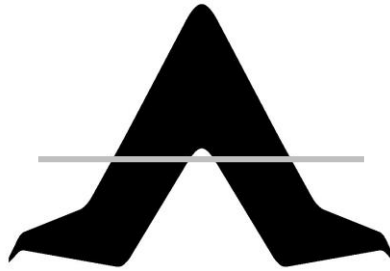


Figure 6.9 – Position of the neutral point of the Flying V planform (little dot) with the center of gravity (big checked dot) 6% MAC in front of it

The center of gravity must be placed in front of the neutral point (see Chapter 3.2.1) to achieve longitudinal stability as required with (3.2).

Then, the wing twist or profile shape has to be chosen in a way that all moments created by aerodynamic forces around the longitudinal axis are balanced for the desired lift.



**Figure 6.10 – For trimmed flight moments around the longitudinal axis running through the center of gravity must be balanced**

However, the pressure distribution has also an impact on the performance (see Chapter 3.1). To minimize the induced drag for a given wingspan, the lift distribution in spanwise direction should be elliptical. This was derived and published by Ludwig Prandtl here [34, p. 32]. It can be applied to this highly swept design due to Munk's theorem stating that the overall induced drag does not depend on the position of the lifting elements in flight direction described in [34, p. 41].

Thus, it is the goal to trim the aircraft as described above with an elliptical lift distribution. Comparing Figure 3.9 and Figure 6.10 one finds that a higher static margin

$$\xi = \frac{x_n - x_{cg}}{MAC} \quad (6.26)$$

can be achieved for high sweep angles and moderate taper ratios than for low sweep angles and higher taper ratios with an elliptical lift distribution.

The influence of the wing sweep for instance can also be illustrated when  $\xi$  is kept constant for an exemplary untapered as well as uncambered wing and this wings sweep is then increased while for every sweep angle its twist is optimized for the lowest induced drag.

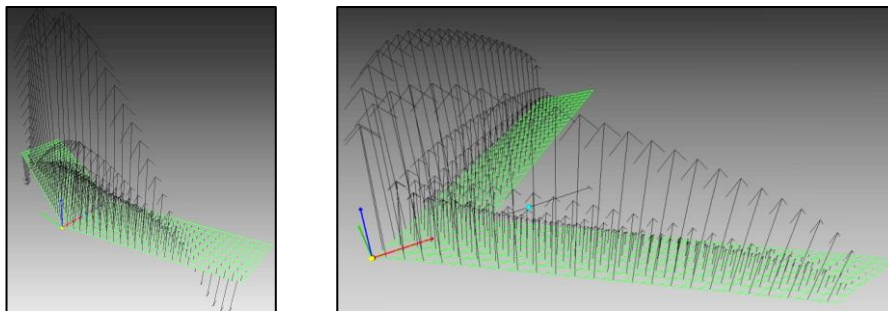


**Figure 6.11 – Untapered wing with different sweep angles optimized for lowest induced drag with a fixed static margin in ODILILA**

One finds that for low sweep angles an elliptical lift distribution cannot be achieved while for higher sweep angles this is possible.

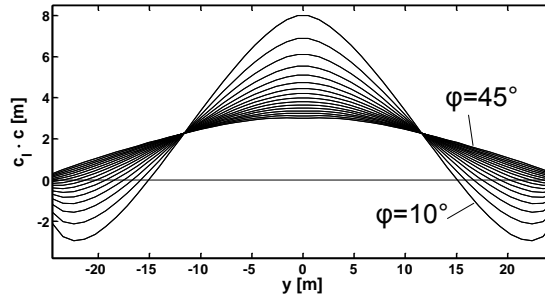


**Figure 6.12 – With higher sweep angles the lift distribution can be closer to the shape of an ellipse for wings with same camber and static margin; wing twist of each wing is optimized for lowest induced drag with ODILILA**

For positively cambered sections sweep the angles when the elliptical lift distribution is reached are higher. For negatively cambered sections or reflex camber lines they are lower.

For the Flying V the wing sweep is set by the cabin with (6.16). Such a wing sweep is too high to trim the aircraft with an elliptical lift distribution for  $\xi \approx 6\%$  when uncambered wing sections are used. The wing must be even more outboard loaded for this case than shown for the highest sweep angles in Figure 6.12.

Extending this highly swept middle wing with tapered transition and outer wings leads to a more elliptical distribution of lift (for the uncambered wing with optimized twist for the lowest induced drag).

The sweep angles  $\varphi_{TW}$  and  $\varphi_{OW}$  as well as the taper ratios  $\lambda_{TW}$  and  $\lambda_{OW}$  of the transition and outer wing have an influence on the lift distribution (thus the induced drag), the absolute position of the neutral point, the wetted area and the wave drag. Their shape is restricted by the requirement that local  $c_l$  values must not exceed critical values.

As a measure to further reduce wetted area also the taper ratio  $\lambda_{MW}$  is introduced as a further variable for the planform. It also has an influence on the ideal lift distribution.

The geometry of the transition and outer wings has not been optimized in this work but selected as a first engineering judgment. The selection will be reviewed in the forthcoming chapters.

The wingspan of the aircraft will be set to the gate limit. Due to the spanloaded design low bending moments are expected (for a detailed analysis see Chapter 6.4.2.1).

$$b = 65m . \quad (6.27)$$

With

$$\varphi_{25,TW} = 53^\circ , \varphi_{25,OW} = 13^\circ , \lambda_{MW} = 0.9 , \lambda_{TW} = 0.38 , \lambda_{OW} = 0.35 , \quad (6.28)$$

kinks at

$$\eta_{TW} = 0.4 , \eta_{OW} = 0.6 , \quad (6.29)$$

and winglets with the geometry of

$$\varphi_{25,WL} = 20^\circ , \lambda_{WL} = 0.3 , \eta_{WL} = 0.95 \quad (6.30)$$

one gets a lift distribution as it is shown here:



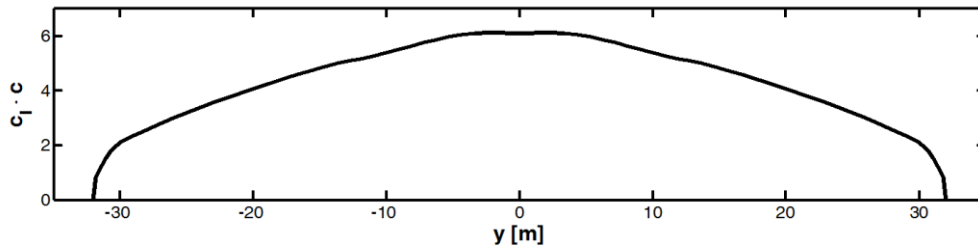


Figure 6.13 – Lift distribution of the Flying V optimized with ODILLA for the geometry set above with a static margin of 6% and uncambered wing sections of the middle wing and wing sections with 2% camber of the transition and outer wings,  $C_L=0.25$

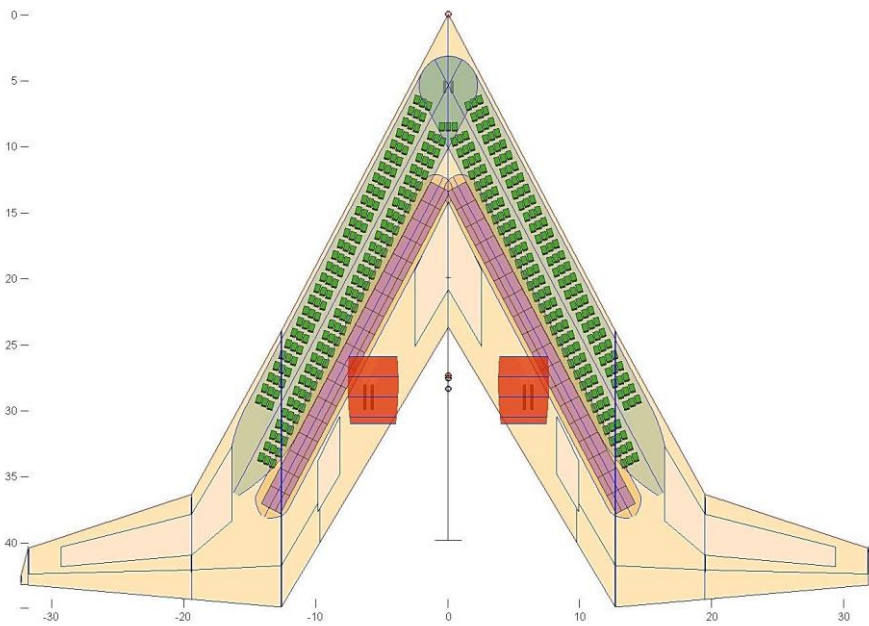


Figure 6.14 – Planform layout with the geometry set above

This lift distribution is achieved with a twist distribution<sup>1</sup> as it is shown on the right. The inner part of the highly swept middle wing induces more and more upwind further to the outside of the middle wing, so the angle of attack of the middle wing sections has to decrease in order to achieve the elliptical distribution of lift giving the middle wing a negative wing twist. The sections twist around the cabin as described with (6.5).

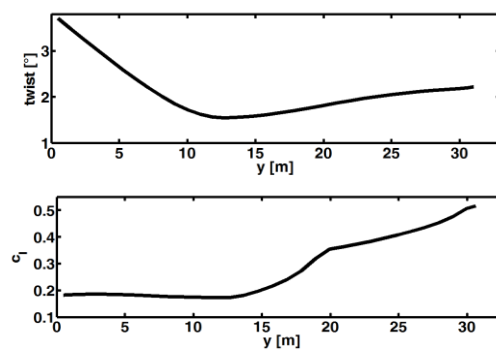


Figure 6.15 – Upper diagram: twist calculated with ODILLA for the lift distribution shown in Figure 6.13, lower diagram: local  $c_l$  values

Due to the highly tapered transition wing the twist even has to slightly increase further all the way to the tip of the outer wing in order to create enough lift locally to achieve the elliptic lift distribution.

<sup>11</sup> It is remarkable how low the twist of the Flying V design is compared to Blended Wing Body designs. The twist range for the Flying V is merely 2° whereas it is roughly 8° for Blended Wing Body designs [35, p. 11].

The optimization was made for a design  $C_L$  of

$$C_{L_{cruise}} = 0.25. \quad (6.31)$$

As a first estimate for the mass of the airplane a slightly lower weight than the maximum take-off weight of the reference aircraft

$$MTOW = 260000kg \quad (6.32)$$

was taken. With a chosen wing area of

$$S = 895m^2 \quad (6.33)$$

this leads to (6.31) for cruise conditions.

The local  $c_l$  distribution can be seen in the lower diagram of Figure 6.15. For the given geometry the local  $c_l$  values of the middle wing are  $<0.2$ . They decrease slightly to the outside of the middle wing although the wing chord also decreases. As the wing chord decreases rapidly at the transition wings the local  $c_l$  values increase. This continues on the outer wing and winglet resulting in a maximum of

$$c_{l,max,cruise} = 0.52 \quad (6.34)$$

at the tip.

The relative profile thickness is set by the chosen geometry. The absolute height of the middle wing is set by the cabin with (6.10), see Chapter 6.2.2.1. The relative profile thickness of the middle wing increases linearly from

$$(t/c)_{MW,i} = 13.5\% \quad (6.35)$$

to

$$(t/c)_{MW,o} = 15.3\% \quad (6.36)$$

on the outside slightly tapering the middle wing. For transition and outer wing the relative profile thickness is not set by the planform and a required absolute height. Due to the higher  $c_l$  values it must decrease though to achieve low wave drag, see Chapter 6.3.5.

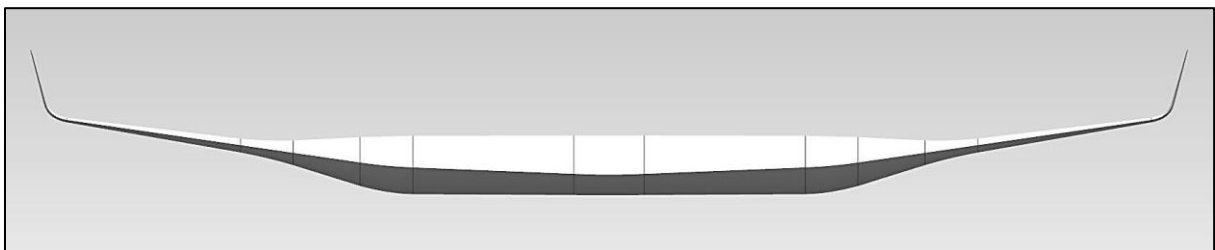


**Figure 6.16 – Lifting body of the Flying V viewed from the back, middle wing with constant absolute height (6.10) twists around the horizontal cabin after (6.5) and with the twist determined in this chapter, airplane is trimmed for cruise flight as it is shown in the picture, kinks are blended in the picture**

Stability as required with (3.2) is fulfilled for the chosen geometry as can be seen in the following diagram.

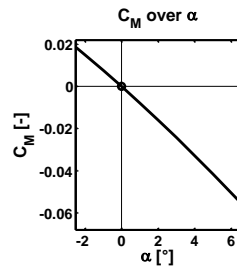


Figure 6.17 –  $C_M$  over the angle of attack of the cabin floor. Aircraft is longitudinal stable after (3.2) and trimmed for  $\alpha=0^\circ$ .

Major design challenges which could be determined designing the basic planform are:

- The relative profile thickness of the middle wing has a direct influence on the wing area. Whereas a smaller relative thickness leads to low local  $c_l$  values and a low wave drag, a high relative thickness reduces wetted area
- Decreasing the taper ratio of the transition and outer wings leaving the middle wing as it is leads to a lower wetted area but increases the local  $c_l$  values, particularly at the wing tips
- Increasing the sweep of the transition and outer wings leads to lower wave drag but moves the neutral point far back increasing the center of gravity movement (this will be assessed in Chapter 6.5.1)
- Cambering the wing sections influences the planform shape with which it is possible to achieve trimmed flight with an elliptical lift distribution

Further studies will be required to optimize the planform shape of the Flying V.

Nevertheless, a longitudinal stable configuration with a low wetted area (see next subchapter) and an almost elliptical lift distribution was found with the geometry chosen above.

The accuracy of the results obtained with ODILILA will be substantiated with a model flying demonstrator which shows perfect flight characteristics built with the exact twist and camber distribution and center of gravity position as calculated with the tool. It will be described further in Chapter 6.6.

### 6.3.3 Performance comparison with the reference aircraft

The reference aircraft is also modeled in ODILILA: The planform geometry is taken from the reference and the wing twist and horizontal tailplane angle of incidence is optimized with ODILILA for lowest induced drag. As mass the **MTOW** is taken. As a result the lift to drag ratio of both aircraft can be compared. Keep in mind that wave drag cannot be computed with the tool.

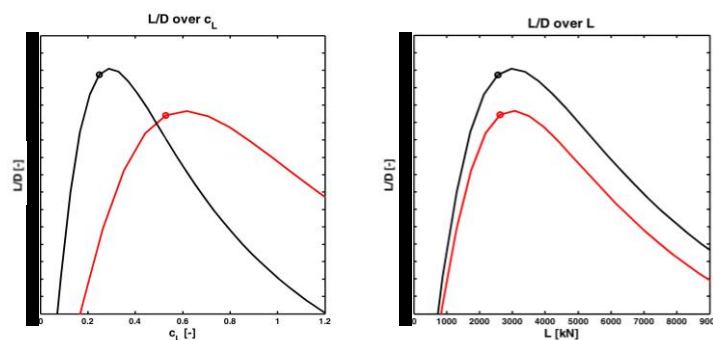


Figure 6.18 – L/D over  $C_L$  and L, black upper line: Flying V, red lower line: A350-900, marked is the design  $C_L$  and the design lift for which the lift distribution of both aircraft has been optimized and for which they are trimmed, curves are then obtained by changing the angle of attack of the aircraft from this point

For the Flying V the lift to drag ratio at the design  $C_L$  is at

$$(L/D)_{cruise, FV} = \blacksquare \quad (6.37)$$

For the reference

$$(L/D)_{cruise, ref} = \blacksquare \quad (6.38)$$

is obtained.

This 10% benefit has two reasons: First, there is a 10% benefit in friction drag due to a lower wetted area of the Flying V. For the chosen geometry it is

$$S_{w, FV} = 2003m^2 \quad (6.39)$$

and for the reference it is

$$S_{w, ref} = 2208m^2. \quad (6.40)$$

(These values include engines (the same for reference and Flying V as a first estimation) and exclude pylons and fairings.)

Second, larger winglets on the Flying V than on the reference (the wingtip chord length on the reference is roughly 1.8m while on the Flying V it is 2.8m offering more room for efficient attachments), a more elliptical lift distribution, and a lower mass lead to a benefit of 18% in induced drag.

The two savings in drag lead to the 10% benefit in L/D.

It shall be emphasised once more that the wetted area (and the wing area) of the Flying V is strongly influenced by the chosen relative profile thickness of the main wing and the cabin height. To evaluate and develop the concept further in forthcoming studies these particular relations and their influence on the overall performance and weight of the aircraft must be studied carefully.

### 6.3.4 L/D for different CG-positions

The movement of the center of gravity will be calculated in Chapter 6.5.1. Here, the change in the L/D for a changed center of gravity position will be given. When the center of gravity moves from its design position flaps have to be deflected changing the lift distribution in a way that the aircraft is trimmed again.

Flaps are installed at the trailing edge of the outer middle wing, the transition wings and the outer wings (see Figure 6.14). Their deflection to counteract a given pitching moment created by an offset of the center of gravity from its design position is optimized for lowest induced drag with ODILILA.

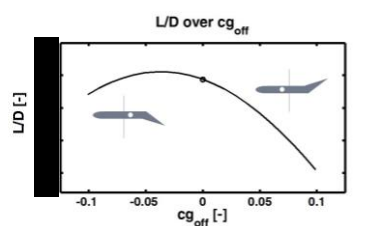


Figure 6.19 – L/D for cruise flight over the center of gravity movement.  $cg_{off}$  is given relative to MAC, for example – a positive  $cg_{off}=0.1$  means that the center of gravity is 10% MAC from the design position, for negative values it is moved to the back

The MAC of the Flying V with the chosen geometry is

$$MAC = 20m \quad (6.41)$$

so a center of gravity movement of 10% is a movement of  $2m$ . The optimum flap deflection determined with the tool for an exemplary 10% movement of the center of gravity to the front is

$$\begin{aligned} fd_1 &= 0.4^\circ, \\ fd_2 &= 1.3^\circ, \\ fd_3 &= 2.1^\circ, \end{aligned} \quad (6.42)$$

where  $fd_1$  is the upwards deflection of the flap on the outside of the middle wing,  $fd_2$  the upwards deflection of the flap on the transition wing and  $fd_3$  the upwards deflection of the flap on the outer wing. These low deflections are possible due to the long lever arm the control surfaces have to the center of gravity (compared to Blended Wing Body type of aircraft (compare [7])). Their neutral point and thus the center of gravity of these type of aircraft lies further to the back compared to the Flying V design.

### 6.3.5 Some notes on the profile design

#### 6.3.5.1 Middle wing

As mentioned in previous chapters the profile shape of the middle wing of the Flying V has a strong influence on the whole aircraft (cabin space, structure, aerodynamics).

At this point in this work, the relative thickness of the profile is given with (6.35) and (6.36). Local  $c_l$  values for cruise flight for the middle wing have been determined in the previous chapter.

In addition to the profile shape and sweep angle, they are the main drivers for wave drag. Higher local  $c_l$  values and higher profile thicknesses lead to higher wave drag (compare [22]).

Local  $c_l$  values and relative profile thickness for the middle wing of the Flying V are below values generally obtained for the center lifting body of Blended Wing Body designs [35, p. 10], [35, p. 11]. Local  $c_l$  values of such designs optimized for low wave drag average around  $c_l \approx 0.23$  at the main wing and the relative profile thicknesses average around  $t/c \approx 16\%$  [35, p. 13]. Wave drag of such configurations is of the same order of magnitude as for conventional configurations [35].

Thus, it can be assumed for purposes of preliminary design that the chosen profile thickness and local  $c_l$  values should not be critical in terms of wave drag.

The maximum thickness location of profiles used for the center lifting body of Blended Wing Body designs is at around 30% [35, p. 11]. This makes it possible to fit a cabin as proposed in chapter 6.2.2.1 close to the leading edge (see Figure 6.24).

However, a numerical study of transonic flow over the Flying V will be necessary to validate these preliminary assumption.

Also, detailed studies will be required to develop the profile shape itself. In the following, a profile will be proposed as engineering judgment and thoughts which lead to the design will be given. Keep in mind though, that the proposed design is only a first sketch.

The basic shape of transonic airfoils was first proposed in 1960 by Richard T. Whitcomb [36].

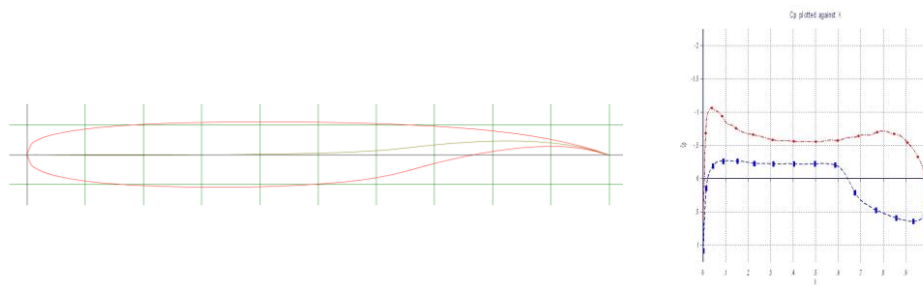


Figure 6.20 – Transonic airfoil and its pressure distribution for  $c_l=0.6$  by Whitcomb at  $Ma=0.75^1$  in VGK<sup>2</sup>

With a big nose radius and a flat upper surface the pressure distribution on the upper side is kept fairly constant. To fit a circular cabin inside the leading edge it is desirable to take a profile with an even bigger nose radius and a maximum thickness position which is further up front to the leading edge. However, a rise of the wave drag due to a shock on the upper surface is likely if this measure is taken, even at low  $c_l$  values (as on the middle wing of the Flying V).

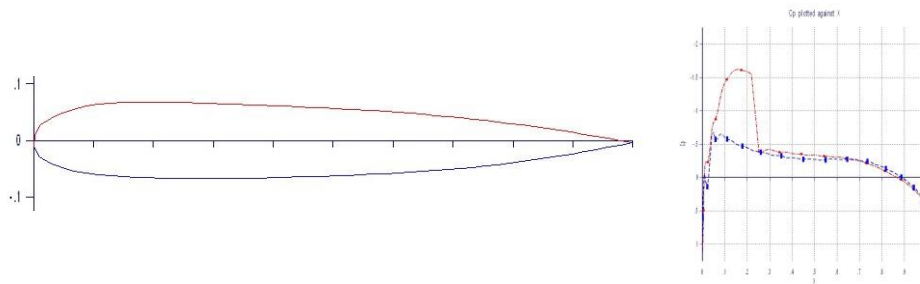


Figure 6.21 – Symmetrical airfoil with big nose radius and a maximum thickness position at 25% by the author for  $c_l=0.2$  at  $Ma=0.75$

The shock does not occur when the shape of the upper surface is changed to the shape of the upper surface of a transonic airfoil (NASA sc 0712). The traditional rear loading of transonic airfoils is not required here because only low local  $c_l$  values have to be achieved. A slight middle loading (see following picture) can help to achieve the required  $c_l$  value and at the same time not create nose down pitching moments as high as with rear loaded profiles. Nose down pitching moments have a negative impact on the lift distribution which is needed to trim the aircraft for the chosen planform geometry of the Flying V.

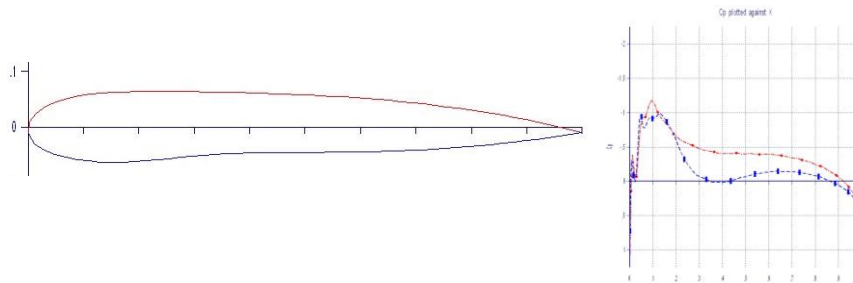
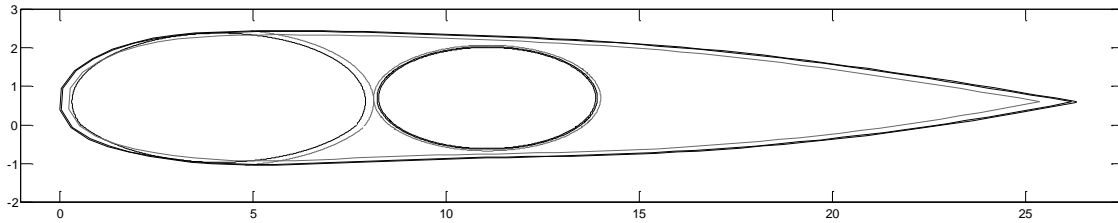


Figure 6.22 – Attempt of an airfoil with a big nose radius and a far up front maximum thickness position without a shock by the author for  $c_l=0.2$  at  $Ma=0.75$

<sup>1</sup> The design tool did not permit any tests at higher Mach numbers

<sup>2</sup> Design tool for transonic wing sections „VGK“ used in the Future Project Office of Airbus

The chosen profile is displayed in the following picture. It is almost symmetrical only with slight modifications that the cabin cross section sits well into the front section. On Blended Wing Body type of aircraft symmetrical sections with a maximum thickness position of 30% are used without the occurrence of a shock for  $c_l = 0.23$ , a relative thickness of 16% and at  $Ma > 0.8$ . [35]. The maximum thickness position of 30% is adopted here.



**Figure 6.23 – Proposed profile in streamwise direction with elliptical cuts for cabin and cargo section, almost symmetrical profile with an upper surface of a transonic profile and a slight middle loading**

Turned  $63^\circ$  the profile can be displayed with the cabin and cargo cross section.

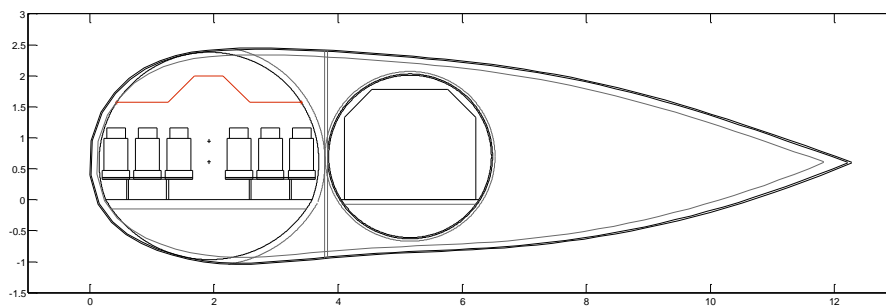


**Figure 6.24 – Cabin and proposed profile**

### 6.3.5.2 Transition and outer wings

For the transition and outer wings the requirement to fit a circular cabin into the front section does not exist. Their detailed profiles were not selected in the scope of this work.

For the chosen geometry the relative profile thickness of the outer wings will have to be low due to the low sweep angle  $\varphi_{25,OW} = 13^\circ$  (6.28). As bending moments are low compared to conventional configurations though (will be shown in Chapter 6.4.2.1) this might still be feasible. Further work will be needed on this topic.

### 6.3.6 Take-off and landing

The maximum angle of attack at take-off and landing follows from the chosen geometry and is roughly

$$\alpha_{takeoff, max} = 12.5^\circ. \quad (6.43)$$

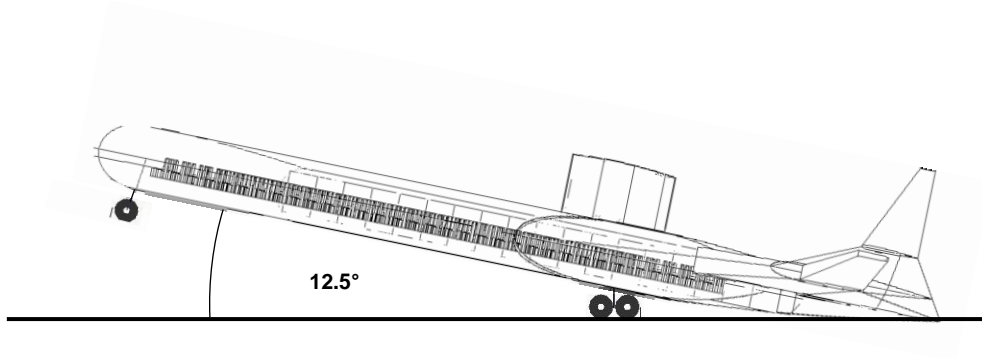


Figure 6.25 – Maximum angle of attack of the Flying V at take-off and landing given by the geometry

Assuming the same speed for take-off like the reference aircraft, roughly

$$v_{takeoff} \approx 150kt \tag{6.44}$$

at ISA+15, the lift coefficient at take-off is

$$C_{L,takeoff} = 0.71 . \tag{6.45}$$

The angle of attack needed to achieve this lift coefficient can be calculated with ODILILA. The low speed polar is given below. It is

$$\alpha_{C_{L,takeoff}} = 8.5^\circ . \tag{6.46}$$

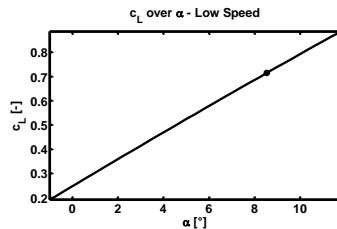


Figure 6.26 –  $C_L$  over  $\alpha$ , low speed, marked is  $C_{L,takeoff}$

The lift to drag ratio for trimmed flight at low speed can be calculated with ODILILA.

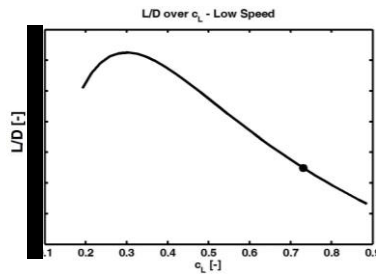


Figure 6.27 –  $L/D$  over  $C_L$ , low speed, marked is  $C_{L,takeoff}$

The flap deflection to trim the aircraft at  $C_{L,takeoff}$  is



$$\begin{aligned}
 fd_1 &= 0.9^\circ, \\
 fd_2 &= 3.2^\circ, \\
 fd_3 &= 5.2^\circ.
 \end{aligned}
 \tag{6.47}$$

At a CG position moved 5% MAC forward of the design position (trimmed cruise flight without flap deflection) the flap deflection at low speed and  $C_{L, takeoff}$  is

$$\begin{aligned}
 fd_1 &= 1.7^\circ, \\
 fd_2 &= 6.2^\circ, \\
 fd_3 &= 10.0^\circ.
 \end{aligned}
 \tag{6.48}$$

Maximum forward CG positions for the chosen design are 5% of MAC as will be shown in Chapter 6.5.1.

The take-off angle for this case is

$$\alpha_{C_{L, takeoff}, CG_{off}=0.05} = 10.1^\circ.
 \tag{6.49}$$

A take-off and landing performance calculation was not done in this work. The following points could be critical:

- Local  $c_l$  values on tips at high angles of attack,  $C_{L, max}$
- Take-off rotation, nose down pitching moment of the engines
- Angle of attack of the cabin floor at approach higher than for conventional configurations

These points should be studied in future work.

## 6.4 MASS EVALUATION

### 6.4.1 Weight breakdown

The weight breakdown of the Flying V and the reference is as follows:

<i>STRUCTURE</i>	
<i>POWER UNITS</i>	
<i>SYSTEMS</i>	
<i>FURNISHINGS</i>	
<hr style="border: 1px solid black;"/>	
<b>MANUFACTURER'S WEIGHT EMPTY (MWE)</b>	
<i>OPERATOR'S ITEMS</i>	
<hr style="border: 1px solid black;"/>	
<b>OPERATION WEIGHT EMPTY (OWE)</b>	

In the following subchapters these groups will be broken down and their weight for the Flying V will be estimated and compared with the reference.

#### 6.4.1.1 Structure

The structure breakdown of the Flying V and the reference are as follows.


<i>STRUCTURE:</i>	<i>Flying V</i>	<i>A350-900</i>
	<i>Pressurized structure</i>	<i>Fuselage</i>
	<i>Middle/transition wings</i>	<i>Wing structure</i>
	<i>Outer wings</i>	<i>Horizontal tailplane / vertical tail</i>
	<i>Landing gear</i>	<i>Landing Gear</i>
	<i>Engine mountings</i>	<i>Engine mountings</i>

The weight of the structure of the Flying V will be estimated in the following.

*Pressurized structure:*

The pressurized structure of the Flying V consists of four cylindrical pressurized sections. **Their weight is estimated by scaling fuselage sections of the A320.**

For the front part of the pressurized cabin section the structural weight of Section 11/12 which is the front section of the A320 is used for scaling (see Figure 6.29). Two of these sections are taken overlapping in the front kink (rough estimate for **additional weight needed in the kink due to the flat pressurized section** in the kink).

For the middle part of the pressurized cabin section (see Figure 6.29) the structural weight of Section 13 of the A320 is used for scaling. **Section 13 of the A320 is located in between Section 11/12 and the fuselage section accommodating the center wing box of the A320.** 

For the rear part the rear section with the pressure bulkhead of the A320, Section 18, is used for scaling.

The sections are scaled in length according to the chosen geometry of the Flying V. More weight must be added to the result because the height ratio of the cabin (6.10) is

$$f_{HR, FlyingV} = 0.95 < f_{HR, A320} = 1. \quad (6.50)$$

Studies of pressurized sections with height ratios  $f_{HR} < 1$  have been made within Airbus:

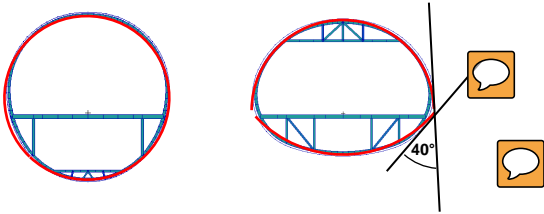


Figure 6.28 – Cross sections investigated by Airbus, circular arcs added by the author, left picture with  $f_{HR}=1$ , right picture with  $f_{HR}=0.75$

Results for the two sections displayed in Figure 6.28 are:

Elements	Weight of flat section elements in percent of circular section elements
Skin	■
Stringers	
Frame	
Framework & crossbeam	

Table 6.1 – Weight increase of the flat section displayed in Figure 6.28 compared with the circular section

For the cross section of the Flying V the angle  $\nu$  which tangents of the circular arcs form at the section with the floor beam is smaller than in the example above (compare (6.9)):

$$\nu_{FlyingV} = 9^\circ < \nu_{Example} = 40^\circ . \tag{6.51}$$

As an estimation, half of the weight increase determined in the example (Table 6.1) will be taken for the three sections of the pressurized cabin structure.

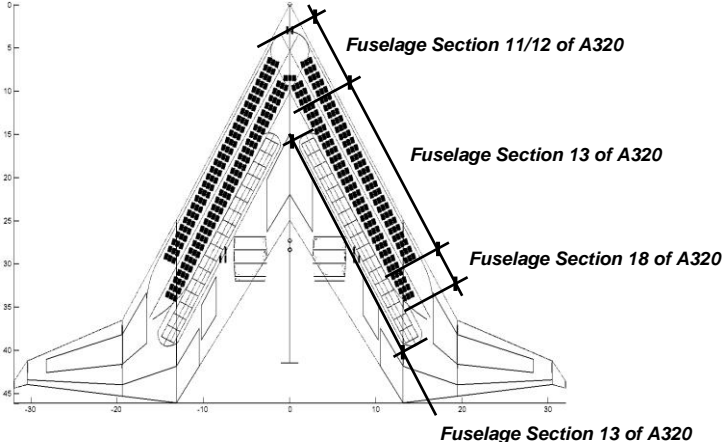


Figure 6.29 – Weight of pressurized structure of the Flying V is estimated by scaling fuselage sections of the A320

For the cargo sections (see Figure 6.29) the structural weight of Section 13 of the A320 is used for scaling. The sections are scaled lengthwise as the cabin sections, but the cargo section is also scaled to a smaller diameter.

Scaling the cargo section weight to a smaller diameter can be achieved by multiplying it with  $d_{cargo}/d_{A320}$  when the same weight per area is taken for both the original and the scaled section. According to the Barlow’s formula (4.2) it is then

$$\sigma \sim d \tag{6.52}$$

for the constant wall thickness  $k$ . To keep  $\sigma = const$  though when reducing the diameter the thickness  $k$  can be reduced. To keep  $\sigma$  constant the model of the Barlow's formula requires that the weight of the has to be multiplied by  $(d_{cargo}/d_{A320})^2$ .

Extra weight due to a flat cross section does not have to be added for the cargo section because it is circular.

With a few additional assumptions<sup>1</sup> one gets the weight breakdown<sup>2</sup> for the pressurized structure:


Pressurized structure of Flying V		Fuselage structure of reference for comparison
Cabin Panels		
Cargo Panels		
Cabin Frames		
Cargo Frames		
Doors		
Windscreen and windows		
Windscreen and opening frames		
Cabin floor structure and framework		
Cargo floor structure		
Special structures		
Miscellaneous		
<b>Total</b>		

Table 6.2 – Pressurized structure of Flying V

*Middle/transition wings*

The weight of the middle wing skin and the transition wing skin is estimated by assuming a skin thickness of

$$t_{MW} = t_{TW} = 4mm . \tag{6.53}$$

For the inner structure of the middle and transition wings a mass is assumed as a starting point. This mass will be recalculated in a second iteration after the wing bending has been calculated.


Middle wing / transition wing structure of Flying V		Wing structure of reference for comparison
Skin		
Inner wing structure		
<b>Total</b>	<b>100%</b>	<b>102%</b>

Table 6.3 – Middle wing / transition wing structure of Flying V, first iteration, not final breakdown

*Outer wings*

The wing area of the outer wings roughly matches the wing area of the A320. As a conservative first estimation the weight of the A320 wings will be adopted for the outer wings of the Flying V.

<sup>1</sup> As a rough estimate for the doors the weight of all doors on the A320 was taken times two. This gives eight passenger doors and four cargo doors. The weight of windscreen and windows was taken from one A320 fuselage because the Flying V will have roughly as many windows as an A320. 25% of the special structures of the A320 fuselage (fuselage wing interface components, horizontal and vertical tail mounting) were taken. Miscellaneous fuselage structure of the A320 was taken times two.

<sup>2</sup> The weight break down of the A350-900 is strictly confidential. Therefore, all weights here must be displayed with relative percentages.


Outer wing structure of Flying V		Horizontal tailplane and vertical tail of reference for comparison
Skin Spars Ribs Fixed leading edge Fixed trailing edge Movable trailing edge Miscellaneous		
<b>Total</b>	<b>100%</b>	<b>40%</b>

Table 6.4 – Outer wing structure of Flying V

*Landing gear, Engine mountings*

The landing gear weight and the weight of the engine mountings has been adopted from the reference for the first mass estimation.

The total weight for the structure of the Flying V after the first iteration is shown in the following table.



STRUCTUR of Flying V		STRUCTURE of reference for comparison
Pressurized structure Middle/transition wings Outer wings Landing gear Engine mountings		Fuselage: Wing: HTP & VTP: 
<b>Total</b>	<b>100%</b>	<b>103%</b>

Table 6.5 – Structure of Flying V, first iteration, not final breakdown

### 6.4.1.2 Power Units, Systems, Furnishings, Operator’s items

The mass of the groups *POWER UNITS, SYSTEMS, FURNISHINGS, OPERATOR’S ITEMS* of the weight breakdown have been adopted from the reference aircraft for the first mass estimation.

The total weight breakdown of the **OPERATION WEIGHT EMPTY (OWE)** of the Flying V after the first iteration is shown in the following table.



OPERATION WEIGHT EMPTY (OWE)		
	Flying V	Reference
STRUCTURE POWER UNITS SYSTEMS FURNISHINGS OPERATOR’S ITEMS		
<b>Total (OWE)</b>	<b>100%</b>	<b>102%</b>

Table 6.6 – Operation weight empty of Flying V, first iteration, not final breakdown

The assessed **OPERATION WEIGHT EMPTY (OWE)** of the Flying V is 2% lower than for the reference. Payload mass  $m_{PL}$  and fuel mass  $m_F$  are adopted from the reference for the design point so (6.32) can be revised.

The influence of this change in weight on the design  $C_L$  taken in Chapter 6.3 is negligible at this stage of the preliminary design.

## 6.4.2 Wing bending and torsion

With the weight breakdown from the last subchapter and the distribution of lift calculated in Chapter 6.3 the loads acting on the structure of the Flying V can be estimated.

### 6.4.2.1 Wing bending

For an estimation of the bending moments  $M_x(y)$  the weight of the Flying V is distributed along the lateral axis. The weight of the *STRUCTURE* and *POWER UNITS* is distributed along the lateral axis after the general layout (Figure 6.14). The weight of *SYSTEMS*, *FURNISHINGS* and *OPERATOR'S ITEMS* is distributed evenly along the lateral axis from tip to tip of the transition wings. The result is a line load of the **OPERATION WEIGHT EMPTY (OWE)** along the lateral axis from wing tip to wing tip  $q_{OWE}(y)$ . The payload is also modeled evenly distributed along the span with boundaries as given by the general layout for a rough estimate. Its line load is  $q_{PL}(y)$ . Fuel is placed in the tanks in the middle, transition, and outer wing as described in Chapter 6.2.4. Its line load is  $q_F(y)$ . The lift distribution was calculated in Chapter 6.3 and its line load is  $q_L(y)$ .

With the line loads the *MTOW* can be displayed cumulatively over the wingspan and the lift distribution can also be shown in the same diagram.

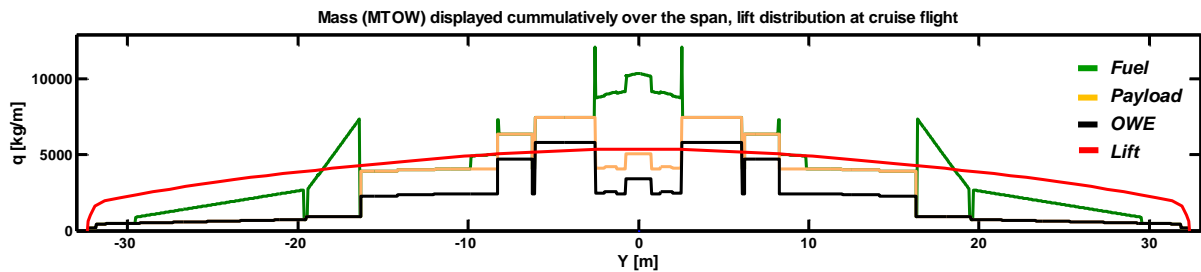


Figure 6.30 – Distribution of mass and lift over the span for the Flying V at MTOW and cruise flight conditions

As critical case an exemplary 2.5g maneuver without fuel is chosen. To model such a case it is

$$q_{M_{2.5g\text{-case}}} = 2.5 \cdot (q_{OWE} + q_{PL}) \quad (6.54)$$

and  $q_{L_{2.5g\text{-case}}}$  is calculated with ODILILA for

$$C_{L_{2.5g\text{-case}}} = 2.5 \cdot C_{L_{cruise}} \cdot \frac{OWE + m_{PL}}{OWE + m_{PL} + m_F} \quad (6.55)$$

1g case with fuel and 2.5g case without fuel are both displayed in the following diagram. The total mass distribution is shown for each case. For the 2.5g case this is given with (6.54) and for the 1g case it is given with

$$q_M = q_{OWE} + q_{PL} + q_F \quad (6.56)$$

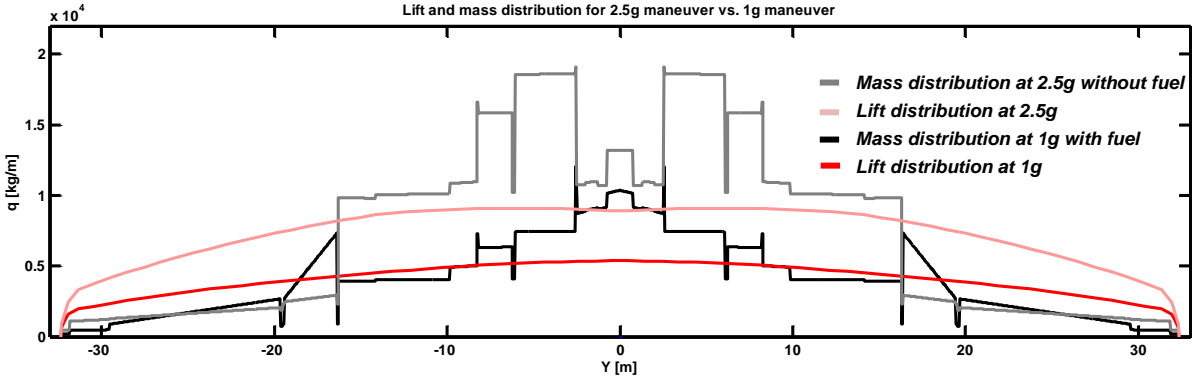


Figure 6.31 – 1g and 2.5g case: spanwise distribution of mass and lift

With  $q_M$  and  $q_L$  the resultant line loading  $q_R$  can be calculated (the following procedure also applies for the 2.5g case)

$$q_R = q_M - q_L \tag{6.57}$$

Then it is

$$\int_b q_R \cdot dy = 0 \tag{6.58}$$

$q_R$  and  $q_{R_{2.5g\text{-case}}}$  are shown in the following diagram.

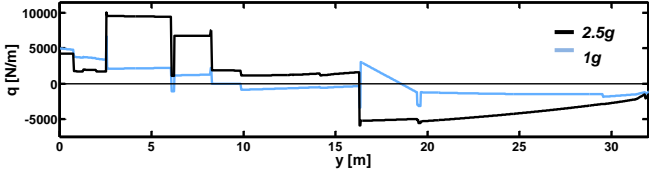


Figure 6.32 – Line loading of the half span of the Flying V

Integrating gives the shear force distribution

$$Q(y) = -\int q_R(y) dy, \text{ boundary condition: } Q(b/2) = 0 \tag{6.59}$$

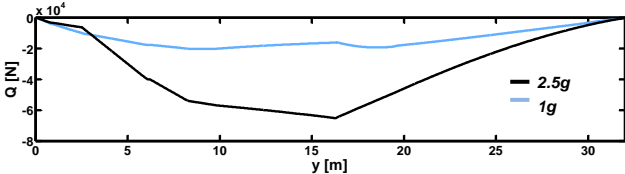


Figure 6.33 – Shear force distribution

Integrating once more gives the moment distribution

$$M_x(y) = \int Q(y) dy, \text{ boundary condition: } M_x(b/2) = 0 \tag{6.60}$$

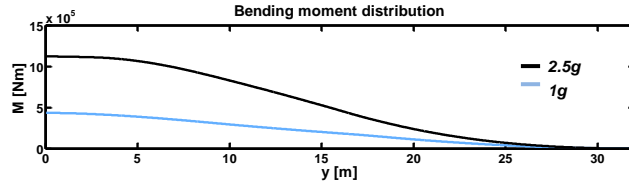


Figure 6.34 – Bending moment distribution

The maximum bending moments can be compared to the maximum bending moments at the wing root of the reference aircraft:

	A350-900	Flying V
$M_{x,max}$	[Redacted]	$11 \cdot 10^5 \text{ Nm}$

Table 6.7 – Maximum bending moments of Flying V and reference

Maximum bending moments are roughly one order of magnitude lower on the Flying V than on the reference. This is due to the spanloaded design.

Due to the low bending moments and the great wing thickness of the middle wing the stress due to bending is low on the Flying V: When the section moment of inertia is roughly estimated with

$$I_{xx} = \int_A z^2 dA \tag{6.61}$$

where  $A$  is the area resulting from the thickened wall ( $k = 4\text{mm}$ ) of each section cut<sup>1</sup> one gets the following moment of inertia distribution<sup>2</sup>

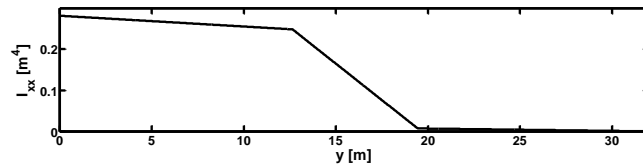


Figure 6.35 – Section moment of inertia distribution

which leads to the maximum stress together with the maximum thickness distribution  $z_{max}(y)$  given by the geometry.

$$\sigma_{max}(y) = \frac{M_x(y)}{I_{xx}(y)} \cdot z_{max}(y). \tag{6.62}$$

<sup>1</sup> Relative profile thicknesses of 10% on the kink of the transition and outer wing and 8% on the outer wing tip have been assumed to make the estimation

<sup>2</sup> Section moment of inertia has only been calculated in the kinks and then linearly interpolated for a rough estimation. The actual distribution in between the kinks would not be linear but slack.



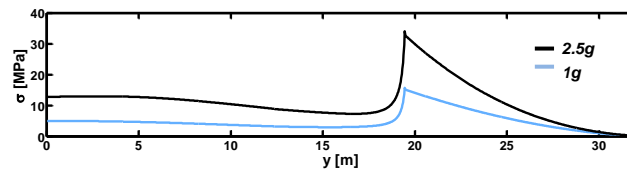


Figure 6.36 – Maximum stress distribution

Wing bending was so far only examined around the longitudinal axis. Due to the high wing sweep it will also be necessary to consider the actual bending of the swept wing around other axis, for instance an axis orthogonal to the leading edge of the middle wing in the x-y-plane.

This was not done in this work. Henceforth it is assumed that the moments in cuts of different angles other than parallel to the longitudinal axis are of the same or a lower magnitude than the moments calculated above. This assumption can be made because the weight of the Flying V is distributed more elliptical along the longitudinal axis than it is along the lateral axis.

#### 6.4.2.2 Wing torsion

The middle wing torsion due to the transition and lower wings of a lower sweep angle can be estimated roughly as shown in the following picture.

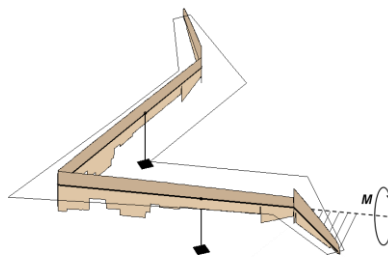


Figure 6.37 – Rough model to estimate the middle wing torsion due to the transition and outer wings of a lower sweep angle

Line loadings calculated in the previous sub-chapter are arranged as shown in Figure 6.37 (at roughly 25% of the chord of the middle wing (rough position of the center of pressure for an uncambered airfoil) and at roughly 50% chord of the transition and outer wings (rough position of the center of pressure for a cambered airfoil)).

The torsion moment for the 1g case is:

$$M_{t,1g} = 1 \cdot 10^5 \text{ Nm} . \quad (6.63)$$

For the 2.5g case it is

$$M_{t,2.5g} = 2.2 \cdot 10^5 \text{ Nm} . \quad (6.64)$$

The torsion moment acting on a conventional A320 fuselage for an engine failure during takeoff can be estimated roughly<sup>1</sup> to be about

$$M_{t,A320,OEI} = 2 \cdot 10^5 \text{ Nm} . \quad (6.65)$$

<sup>1</sup> Consider a short range aircraft with a mass of 78t taking off with one engine at an L/D of 8. Roughly 85kN of thrust must be generated by the engine located roughly 6m away from the center axis. The force counteracting this moment generated by the vertical tailplane roughly 17m behind the center of gravity must then be roughly 30kN. With a lever arm of roughly 4m a moment of 135kNm is created. This is the moment roughly needed for static flight. With a factor of 1.5 for maneuverability the maximum moment is 200kNm.

$M_{t,2.5g}$  and  $M_{t,A320,OEI}$  are roughly of the same magnitude. The structure of the Flying V absorbing this moment is, however, not only the pressurized section but also the whole middle wing structure.

More dimensioning loading scenarios for wing torsion (asymmetric gusts, asymmetric landing, internal wing torsion due engine and landing gear position) will have to be considered in future studies on the Flying V.

Keep in mind though that there is no torsion in the x-z-plane in the middle kink of a swept pure flying wing in static flight.

### 6.4.3 Weight estimation the inner wing structure of the middle and transition wing

In Chapter 6.4.1.1 a **weight of 13000kg** was assumed for the inner wing structure of the middle and transition wing. It shall be recalculated in this chapter.

#### 6.4.3.1 Scaling

The structure will be scaled up from the structure of the reference using three dimensioning cases.<sup>1</sup>

##### Case 1: Aerodynamic Loads

In this case the aerodynamic loads lead to a bending of the skin of the wing. The maximum stress due to this bending is calculated at the root of the A350 to have a reference, then it is calculated for the middle wing of the Flying V.

The **wing loading** of the Flying V (assumption:  $2200N/m^2$ ) is lower than on the A350 (assumption:  $6000N/m^2$ ), so it can be expected, that with the same skin thickness the ribs can be moved further away from each other than on the A350.

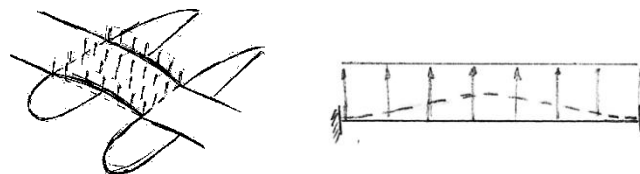


Figure 6.38 – Simplified model for the aerodynamic loads

The model for this is a simple loaded surface which is further be simplified to a beam [24]

$$\sigma_{\max} = \frac{1}{24} ql^2 \cdot \frac{k/2}{I}, \quad (6.66)$$

where  $q$  is the line loading derived from the wing loading,  $l$  is the rib distance,  $k$  is the skin thickness and  $I$  is the skin moment of inertia.

With the same skin thickness, the same maximum stress is achieved when:

Rip distance A350:                      0.6 m

Rip distance Flying V:                1.1 m

---

<sup>1</sup> The author is aware that the following method can be challenged easily. However, it is the best which could be done in the scope of this work to get a very rough estimate of the structural weight.

**Case 2: Buckling of the skin due to wing bending**

In this case the buckling of the skin due to bending of the wing is considered. It is expected that the ribs can be moved further away from each other because the bending moments on the Flying V (assumption:  $10 \cdot 10^5 Nm$ ) are significantly lower than on the A350 (assumption:  $150 \cdot 10^5 Nm$ ).

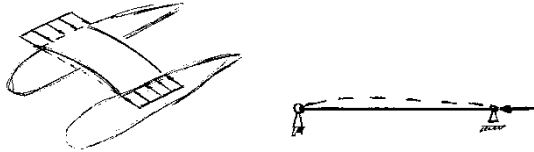


Figure 6.39 – Simplified model of the buckling of the skin due to wing bending

The model for this is a simple loaded surface which is further simplified to a column [24]

$$F_{crit} = \pi^2 \cdot \frac{EI}{l^2} \tag{6.67}$$

where  $F_{crit}$  is the critical force due to bending. When (6.68) is solved for the skin thickness  $k$  (which is given with  $I$ ) the rib distance  $l$  is

Rip distance A350: 0.6 m

Rip distance Flying V: 6.0 m

so that the skin thickness  $k$  is the same for both cases.

**Case 3: Buckling of the ribs due to wing bending**

In this case, the buckling of the ribs due to compression as a result of wing bending is considered.

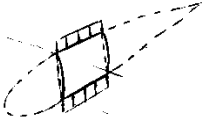


Figure 6.40 – Simplified model of the compression of the wing ribs due to wing bending

The compression can be modeled roughly by the compression of the oblique beams in a framework such as it is displayed in the following picture.

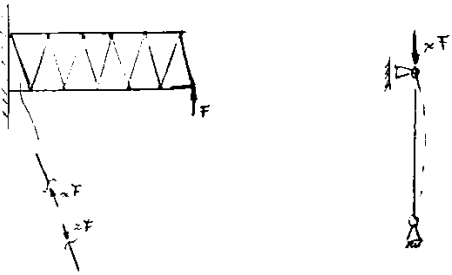


Figure 6.41 – Compression and buckling of beams in a framework

The ratio of the bending moments of Flying V and reference (assumption:  $10 \cdot 10^5 Nm / 150 \cdot 10^5 Nm = 0.07$ ) is modelled by a ratio of the forces  $F$  at the same lever arm. The absolute value of the bending moments does not affect the outcome of this estimation method, only the ratio of the bending moments.

Thus, one has to compare two buckling problems with forces chosen at the ratio 0.07.

A higher required thickness of the ribs will be expected for the Flying V because the height of the ribs of the Flying V (assumption:  $h = 3.4$ ) is greater than the height of the ribs of the reference (assumption:  $h = 1.25$ ), making buckling more likely. A lower required thickness will be expected because the bending of the Flying V is a lot lower than the bending of the reference wing resulting in a lower pressure on the ribs.

The thickness ratio outcome is:

Ratio "rib thickness Flying V" / "rib thickness A350" = 54%.

### **Conclusion**

Case 1 and Case 3 are the most challenging. Case 2 is not dimensioning.

From this rough estimation it seems, that ribs can roughly be placed at twice the distance of the ribs on the reference in the region close to the center axis.

Also, ribs on the Flying V can be twice as thin close to the center axis as on the reference.

Note that the thickness of the ribs might be able to even decrease to the outside on the Flying V because the bending moments get lower, the thickness stays the same though.

The rib distance will not be able to increase because the aerodynamic loads are roughly the same all over the middle wing.

### **6.4.3.2 Weight estimation**

With a rough idea on how the structure of the thick wing of the Flying V scales from the reference the weight for the middle and transition wing can now be estimated.

With the weight of the inner wing structure of the reference and the wing volume of the reference a density of the inner wing structure of the reference follows. The volume of the middle and transition wings of the Flying V has a certain weight if this density of the reference was assumed. With the assumption that the whole inner wing structure scales like the ribs (see previous chapter) it follows that this weight has to be divided by four (Flying V has twice the rib distance and half the rib thickness). The rough estimate for the inner wing structure of the Flying V can thus be revised (see the following table).

#### **To be conservative:**

- This estimation does not take into account that there is already structure available inside the middle wing due to the pressurized sections and cargo sections
- This estimation does not consider that the rib thickness on the Flying V can decrease to the outside due to lower bending than in the center

Middle wing / transition wing structure of Flying V		Wing structure of reference for comparison
Skin		
Inner wing structure		
<b>Total</b>	<b>100%</b>	<b>103%</b>

**Table 6.8 – Middle wing / transition wing structure of Flying V, second iteration**

This leads to the revised breakdown for the structure:

STRUCTUR of Flying V		STRUCTURE of reference for comparison
Pressurized structure		Fuselage:
Middle/transition wings		Wing:
Outer wings		HTP & VTP:
Landing gear		
Engine mountings		
<b>Total</b>	<b>100%</b>	<b>104%</b>

**Table 6.9 – Structure of Flying V, second iteration**

Keep in mind:

- Synergy of fuselage and wing not used in weight assessment
- A320 wing assumption for outer wings conservative due to low bending and no high lift devices
- Engine mounting attachment and landing gear supports not sized and only adopted from the reference

And this leads to the revised total weight breakdown:

OPERATION WEIGHT EMPTY (OWE)		
	Flying V	Reference
STRUCTURE		
POWER UNITS		
SYSTEMS		
FURNISHINGS		
OPERATOR'S ITEMS		
<b>Total (OWE)</b>	<b>100%</b>	<b>102%</b>

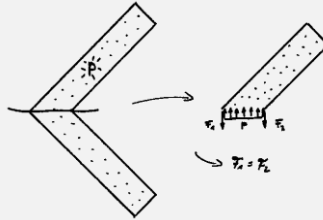
**Table 6.10 – Operation weight empty of Flying V, second iteration**

It shall be emphasised once more here that only the structural weight was assessed, other groups have been adopted from the reference for the rough estimation.

The result of this preliminary mass estimation is that the Flying V has a 2% benefit in mass over the reference. Further and more sophisticated studies are needed to verify this result. This includes the design of an actual structure of the Flying V. This is recommended for future work.

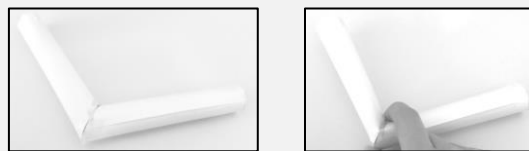
**Does the kinked fuselage bend outwards when put under internal pressure?**

A question which was addressed by many people was if the two connected fuselages would bend outwards because of internal pressure. This, so was their intuition, would lead to significant and sizing bending moments in the connection area. However, a simple free body diagram of a simplified 2D problem illustrates that outward bending will not occur.



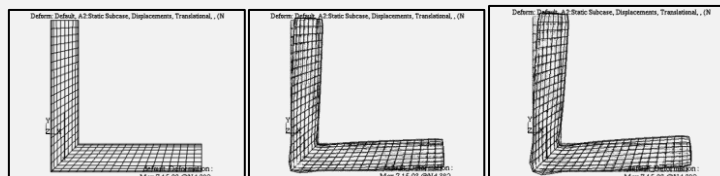
**D2 free body diagram to illustrate that no bending occurs in the kink of a kinked fuselage**

The real 3D problem is difficult to analyze analytical. However it is easily illustrated with a paper model, that the elliptical section in the middle where both parts are connected causes the fuselages to bend a little bit closer together as the section seeks to become circular when put under pressure:



**Deformation of two connected cylinders when the middle elliptical section is pressed circular**

A numerical simulation proves this:



**Deformation of two connected cylinders under internal pressure**

The important point here is that the magnitude of the inward bending does not depend on the length of the circular fuselages. It is only depended on the height ratio of the elliptical section in the connection point, that is to say, the sweep of the fuselages.

**Figure 6.42 – Additional information on the bending of a pressurized kinked fuselage**

## 6.5 HANDLING QUALITIES ASSESSMENT

### 6.5.1 CG diagram for loading

The weight of the *STRUCTURE* and *POWER UNITS* is distributed along the longitudinal axis after the general layout (Figure 6.14). The weight of *FURNISHINGS* and *OPERATOR'S ITEMS* is distributed evenly along the longitudinal axis along the whole range of the cabin and the weight of the *SYSTEMS* group is distributed evenly along the longitudinal axis along the whole aircraft.

With

$$x_{cg} = \frac{\sum (x_{cg,i} \cdot m_i)}{\sum m_i} \quad (6.69)$$

the center of gravity of the **OPERATION WEIGHT EMPTY (OWE)** is determined. To display the maximum center of gravity range a load and balance diagram is drawn:

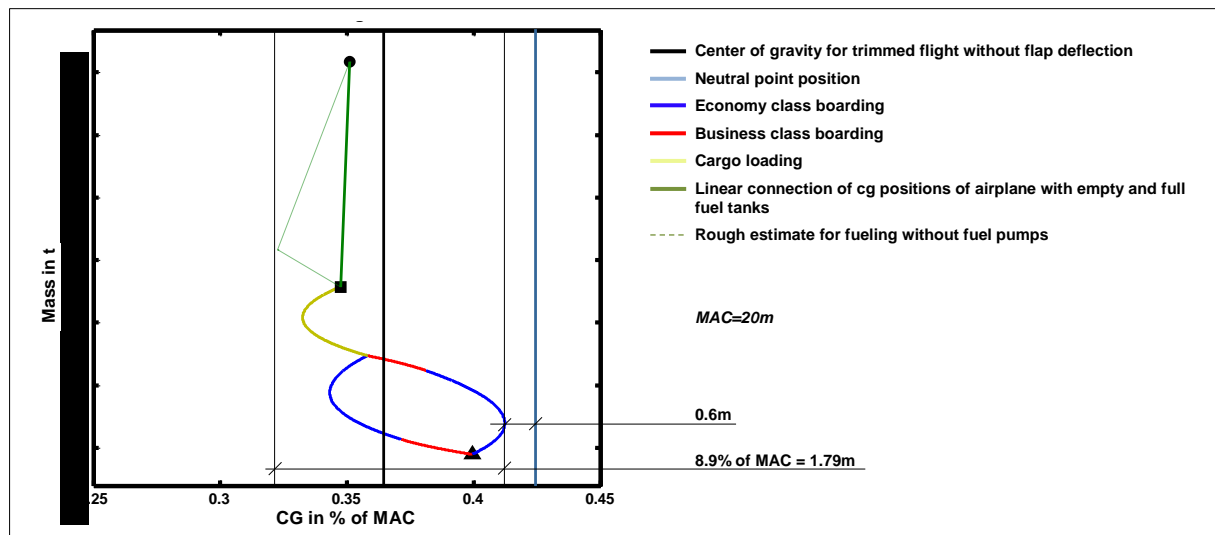


Figure 6.43 – Center of gravity diagram

CG positions are displayed in percent of MAC. The CG position at OWE is displayed with (▲).

The CG position for which the aircraft is trimmed with no flap deflection at cruise flight is shown with the bold black vertical line.

The neutral point position is displayed with the bold blue vertical line.

Passenger boarding is displayed in from the front and from the back. The business class (red line) is placed in the front of the cabin sections. Cargo is loaded in the aircraft from the back. The **MZFW** is displayed with (■).

For filling the fuel tanks the center of gravity position of full and empty fuel tanks are connected with a straight line as a rough estimate. The **MTOW** is displayed with (●).

When no fuel pumps are used the center wing tank is filled up to roughly a half before the transition and outer wing tanks are being filled. This is estimated with the dashed line the outmost point being the center of gravity when the center fuel tank is filled to a half.

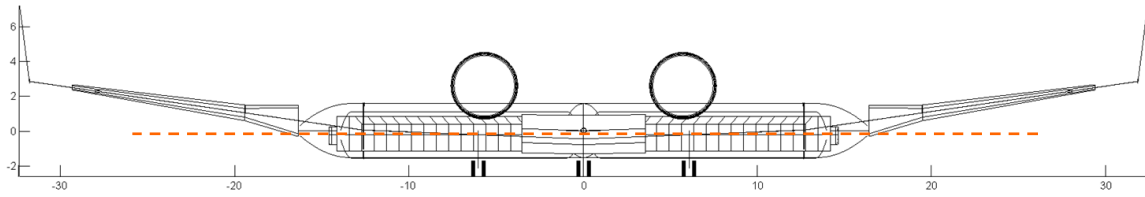


**Figure 6.44 – Rear view of Flying V: half of the center fuel tank is fueled before the transition and outer fuel wing tanks start to be fueled when no fuel pumps are installed**

When the CG diagram in Figure 6.44 is compared with the aerodynamic performance at CG movement in Figure 6.19 one finds that for the most forward center of gravity position in the CG diagram the  $L/D$  in cruise flight goes down 2% (from 25 to 24.5). Flap deflections calculated with ODILILA are below  $1^\circ$  to trim for this case.

Flap deflections to trim the most forward center of gravity positions at low speed at take-off and landing are given in Chapter 6.3.6.

### 6.5.2 Directional stability – simulation

No substantial analysis of the lateral handling qualities is made in the scope of this work. It is, however, desirable to find out if the design is directionally stable at all.

First quick paper models show that the design is directionally stable with a slight dihedral of the outer wings.

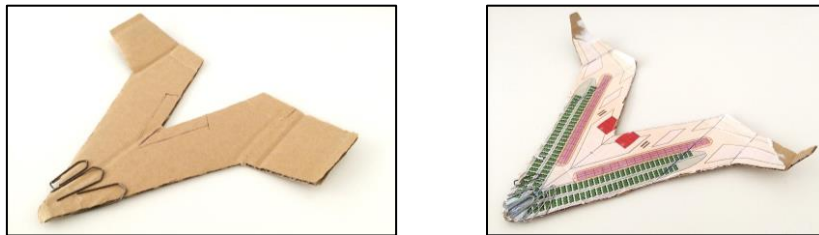


**Figure 6.45 – Very first quick paper model of the Flying V and more refined paper model of the Flying V, the models fly well and directionally stable with a slight dihedral of the outer wings**

It is therefore reasoned that the design can be made directionally stable with a sufficient dihedral of the transition and outer wings and a sufficient winglet size.

A quick simulation of the lateral movement of the airplane shows this as well:

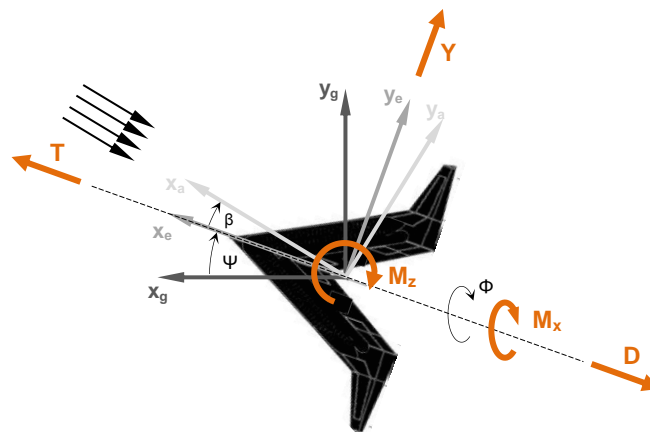


**Figure 6.46 – Flight mechanic model for the movement of the Flying V in the x-y plane,  $\Phi=0$  for horizontal flight**



For small  $\beta$  the equations of motion are simply

$$\begin{aligned} m\ddot{x}_g &= -Y \sin(\Psi), \\ m\ddot{y}_g &= Y \cdot \cos(\Psi), \\ \Theta_{xx} \ddot{\Phi} &= M_x, \\ \Theta_{zz} \ddot{\Psi} &= M_z, \end{aligned} \quad (6.70)$$

where

$$\begin{aligned} Y &= \left[ C_{Y\beta} \cdot \beta + C_{Yp} \cdot \dot{\Phi} \cdot \frac{l_\mu}{V} + C_{Yr} \cdot \dot{\Psi} \cdot \frac{l_\mu}{V} + C_L \cdot \sin(\Phi) \right] \cdot q \cdot S, \\ M_x &= \left[ C_{M_x\beta} \cdot \beta + C_{M_xp} \cdot \dot{\Phi} \cdot \frac{l_\mu}{V} + C_{M_xr} \cdot \dot{\Psi} \cdot \frac{l_\mu}{V} + C_{M_x\eta} \cdot \eta \right] \cdot q \cdot S \cdot l_\mu, \\ M_z &= \left[ C_{M_z\beta} \cdot \beta + C_{M_zp} \cdot \dot{\Phi} \cdot \frac{l_\mu}{V} + C_{M_zr} \cdot \dot{\Psi} \cdot \frac{l_\mu}{V} + C_{M_z\eta} \cdot \eta \right] \cdot q \cdot S \cdot l_\mu, \end{aligned} \quad (6.71)$$

and

$$\begin{aligned} V &= \left( \dot{x}_g^2 + \dot{y}_g^2 \right)^{\frac{1}{2}}, \\ \beta &= \arctan\left(\frac{\dot{y}_g}{\dot{x}_g}\right) - \Psi. \end{aligned} \quad (6.72)$$

Derivatives are determined with ODILILA for cruise flight. Mass moments are estimated with the mass moments of inertia of a simple beam of the same weight. When (6.72) is inserted in (6.71) and (6.71) is then inserted in (6.70) there are four equations for the four unknowns  $x(t)$ ,  $y(t)$ ,  $\Psi(t)$  and  $\Phi(t)$ .

With

$$\begin{aligned} \dot{\xi}_{n+1} &= \ddot{\xi}_n \cdot \Delta t + \dot{\xi}_n, \\ \xi_{n+1} &= \dot{\xi}_{n+1} \cdot \Delta t + \xi_n \end{aligned} \quad (6.73)$$

where  $\xi$  stands for either  $x$ ,  $y$ ,  $\Psi$  or  $\Phi$ , the movement can be simulated with given start conditions  $\xi_0$  and  $\dot{\xi}_0$ .

According to the simulation model, a Flying V design with the chosen geometry and with no dihedral of the transition and outer wings and no winglets is unstable.

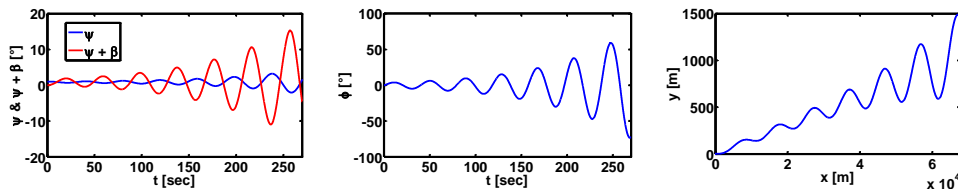


Figure 6.47 – Flying V with no dihedral of transition and outer wings, disturbance:  $\beta=-1^\circ$ , cruise flight

A dihedral of the transition and outer wings of

$$v_{TW} = v_{OW} = 6^\circ \quad (6.74)$$

was chosen. In addition, winglets of a total area (both winglets) of

$$S_{WL} = 16m^2 \tag{6.75}$$

are chosen.

Then the system is stable:

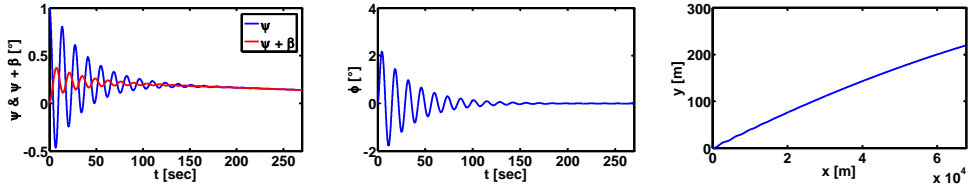


Figure 6.48 – Flying V with 6° dihedral on transition and outer wings and 16m<sup>2</sup> (total) winglets

The dihedral has, however, not only an influence on directional stability. It also influences the center of gravity movement due to fuel consumption (as addressed in the previous chapter) and the feasibility of loading and unloading cargo through rear loading ramps.

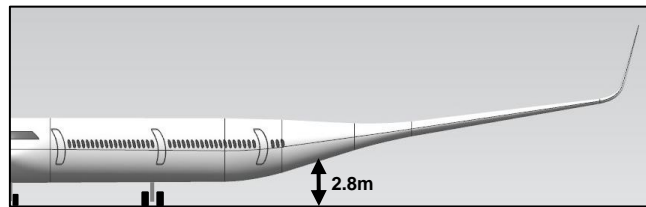


Figure 6.49 – Available height for rear loading ramps to load and unload cargo containers at a dihedral of the transition and outer wings of 6°



## 6.6 RADIO CONTROLLED DEMONSTRATOR MODEL OF THE FLYING V

For demonstration purposes and as validation for the results obtained with ODILILA a radio controlled aircraft of the Flying V was built.

The parts for the wings were cut out of styrofoam:

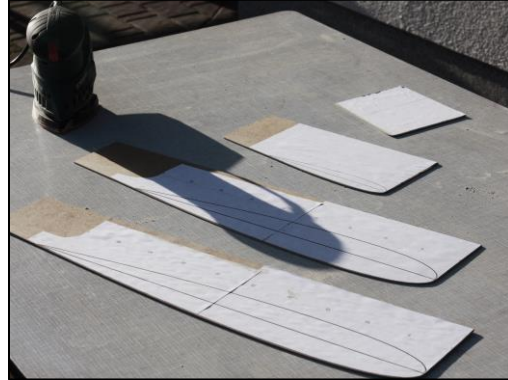


Figure 6.50 - Blocks for the wing elements were cut with a hot wire cutter and the profiles were cut out of wood.



Figure 6.51 - The profiles were arranged at the calculated position with the calculated twist and the wing shape was made with the hot wire cutter as an even ruled surface.

Then the parts were arranged as the Flying V:



Figure 6.52 – The wings were glued together with styrofoam glue and smoothed with sand paper. The flaps were cut out and the model was covered in a thin layer of glass fiber.

The model was equipped and tested in preparation for its first glider flight:



Figure 6.53 – Two servos were installed to actuate the flaps. The battery was installed in the front to place the center of gravity to the calculated position.



Figure 6.54 – The glider model weighs 770g and has a wing area of 0.43m<sup>2</sup>. To achieve the design  $C_L=0.25$  a speed of roughly 40km/h is required. After first slower tests with running the model was brought up to 40km/h with a car. The rudders were tested and the model seemed well trimmed for a neutral flap position at this speed and stable.

The first glider flight was made after throwing the model airplane from a hill:



Figure 6.55 – The model was thrown from a little hill out of a height of roughly 3.5m. After a short and fast decent to gain speed after the throw a straight glide path could be taken up on which the Flying V flew roughly 90m. The airplane was easy to control and landed smoothly.

As next steps engines were installed on the model to demonstrate longer flights with more sophisticated maneuvers.

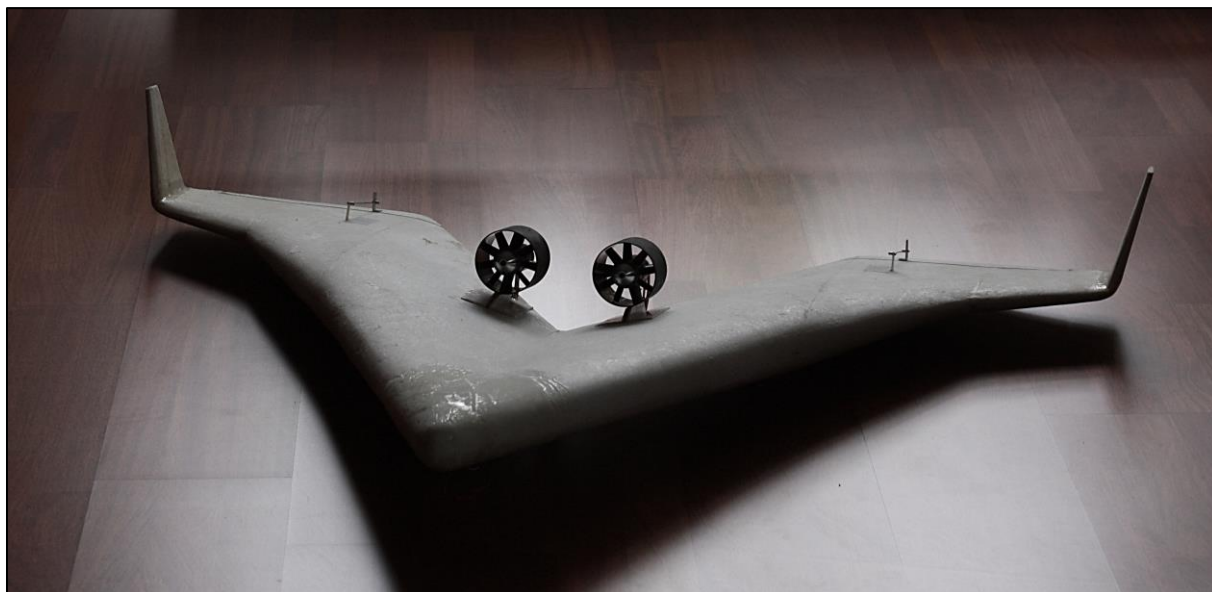


**Figure 6.56** – With the engines and batteries the weight of the model was increased to 1400g. The required speed for the design  $C_L$  is then 50km/h. As engines electro impellers were taken. The batteries were installed in the underbelly.

The test pilot was an experienced pilot for model airplanes and reported that the Flying V model was easy to fly.



**Figure 6.57** – RC model of the Flying V with two birds in the background



**Figure 6.58 – RC model of the Flying V making a sharp turn**

The test pilot could fly sharp turns without difficulties. Also a roll was possible. A stall test was also performed. After the angle of attack was increased further and further and the speed was reduced the nose of the Flying V fell suddenly back down again and the model recovered.

The landing was smooth.



**Figure 6.59 – RC model of the Flying V on final approach for landing**

## 7. CONCLUSION

In this work a new idea on how to efficiently use the volume inside a pure flying wing for commercial passenger transport was derived and a configuration proposal was made with this idea. The configuration was then compared with a reference aircraft.

The idea was to arrange two cylindrical pressurized sections for the payload swept back in the shape of a V and place them inside the front section of a wing with the same sweep angle.

The streamwise cut through the oblique pressurized section is elliptical and efficiently fits into conventional airfoils. The cut of the pressurized section orthogonal to the leading edge is circular leading to an efficient structural solution as pressure can be preserved well in a cylindrical shape.

The proposed configuration is called the Flying V. For this configuration transition and outer wings extend the span of the highly swept middle wing at a lower sweep angle to 65m. The Flying V was designed in this work with a capacity of 315 passengers in a two class layout.

The Airbus A350-900 has the same capacity and was chosen as a reference aircraft. Preliminary estimations made in this work indicate that the Flying V might have a benefit over the reference in terms of aerodynamics (10% higher L/D) and mass (2% lower empty weight).

Further work will be needed to confirm this benefit. A structure will have to be designed for the aircraft to assess the mass of the aircraft more detailed and the aerodynamics have to be assessed in greater detail as well (e.g. estimation of the wave drag, examination of 3D effects, assessment of low speed aerodynamics ( $C_{L,max}$ )). Also, a thorough take-off and landing calculation is needed (exemplary points of interest: take off rotation, bank angles, engine failure, cross wind landing).

Apart from a potential benefit in aerodynamics qualitative arguments in favor of the Flying V which could be derived are the compactness and simplicity of the configuration (less parts, no high-lift devices, no fairings, straight lines) and the shielding of the engines from the ground (low noise).

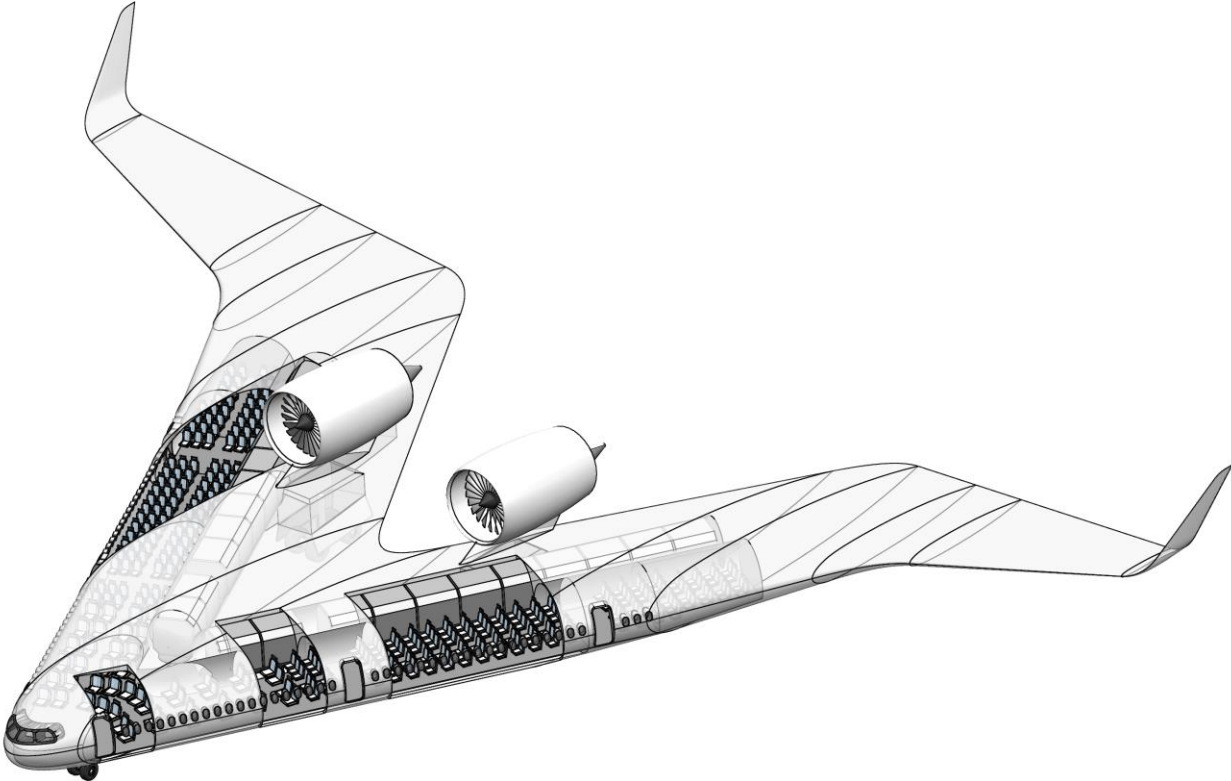
Remarkable is the elliptical lift distribution of the stable design using only a moderate wing twist and no reflexed camber lines. A radio controlled model of the Flying V was presented in this work to demonstrate these aerodynamic characteristics and support the estimations and simulations which were made.

Ways to evacuate the configuration in case of an emergency have to be studied carefully in future work. Current certification regulations may not be applicable for the proposed concept and the actual critical cases have to be examined.

Future work is not only recommended on the final configuration of this work. Especially the position of the cargo compartments, the fuel tanks, and the engines may be subjected to some further studies. Also, the general size and capacity of a Flying V configuration will be interesting to study further. This includes studies on how to realize a family concept with this kind of configuration.

So far, the Flying V is an idea. Everything which was presented in this work can be regarded as the first step of a long iteration which will be necessary to develop the concept further.





## References

- [1] R. Storck, *Flying Wings, Die historische Entwicklung der Nurflügelflugzeuge der Welt*, Bonn: Bernard & Graefe Verlag, 2003.
- [2] Aviation Media & IT GmbH, „Seit 50 Jahren fliegen Boeing-Jets für die Deutsche Lufthansa,“ *aero.de - Luftfahrt Nachrichten*, 2014. [Online]. Available: [http://www.aero.de/content/pics/p\\_669.jpg](http://www.aero.de/content/pics/p_669.jpg).
- [3] Airbus S.A.S., „Airbus Global Market Forecast 2011-2030, Delivering the Future,“ 2011. [Online]. Available: [www.airbus.com/gmf](http://www.airbus.com/gmf).
- [4] E. Torenbeek, *Synthesis of Subsonic Airplane Design*, Delft: Delft University Press, 1982.
- [5] C.-P. Gross, Interviewee, *Airbus Structure Expert on VELA Project*. [Interview]. 2014.
- [6] J. M. Serra, *Preliminary Unconventional Aircraft Design, Short Range Blended Wing Body Aircraft*, Toulouse, 2013.
- [7] Royal Aeronautics Society, „New Aircrafts Concepts Poster,“ 2009. [Online]. Available: [www.raestoulousebrach.org/pastevents/lecturematerial2009/raestlsposterapril09.pdf](http://www.raestoulousebrach.org/pastevents/lecturematerial2009/raestlsposterapril09.pdf).
- [8] P. Wellnhofer, *The illustrated encyclopedia of pterosaurs*, New York: Crescent Books, 1991.
- [9] SuperCrit LLC, „The stomping land,“ 2013. [Online]. Available: [www.thestompingland.com](http://www.thestompingland.com).
- [10] O. Lilienthal, *Der Vogelflug als Grundlage der Fliegekunst*, Berlin: R. Gaertners Verlagsbuchhandlung, 1889.
- [11] F. Saysell, „France, Wordpress Page,“ 2010. [Online]. Available: [www.fatimasaysell.com/category/2010-trips/france/page/2/](http://www.fatimasaysell.com/category/2010-trips/france/page/2/).
- [12] B. Schmidtler, „Statische Längsstabilität,“ *Ultraleichtflug Schmidtler*, 2014. [Online]. Available: [http://www.schmidtler.de/html/ht\\_technik/fm1.htm](http://www.schmidtler.de/html/ht_technik/fm1.htm).
- [13] C. H. Gibbs-Smith, *Clément Ader: his flight-claims and his place in history*, London: H.M.S.O., 1968.
- [14] E. T. Wooldridge, „Century of flight, History of the flying wing, Early flying wings,“ 2014. [Online]. Available: <http://www.century-of-flight.net/Aviation%20history/flying%20wings/Early%20Flying%20Wings.htm>.
- [15] G. Sousmark, „Danmarks Flymuseum,“ 2014. [Online]. Available: [www.flymuseum.de/malerier](http://www.flymuseum.de/malerier).
- [16] R. A. Rolfe, „Macrozania Macrocarpa,“ in *Bulletin of Miscellaneous Information*, Royal Botanic Gardens, Kew, Springer, 1920, pp. 197-199.
- [17] „Alsomitra Macrocarpa,“ International Society of Horticultural Science, 2013. [Online]. Available: [www.cucurbit.org/family/species/Alsomitra/images/macr.jpg](http://www.cucurbit.org/family/species/Alsomitra/images/macr.jpg).
- [18] „Igo Etrich,“ Plant Biomechanics Group Freiburg und Kompetenztechnik Biomimetik, 2013. [Online].

Available: [www.bionik-vitrine.de](http://www.bionik-vitrine.de).

- [19] J. Benad, Entwurf und Windkanaltest eines aerodynamisch stabilen Nurflüglers für den Linienflug, Rostock, 2010.
- [20] „Flying Wings: An Anthology: René Arnoux,“ CTIE, 2002. [Online]. Available: <http://www.ctie.monash.edu.au/hargrave/arnoux.html>.
- [21] D. Bullard, „The Development of All-Wing Aircraft, John K. Northrop,“ 2003. [Online]. Available: [www.nurflugel.com/Nurflugel/Northrop/northrop.html](http://www.nurflugel.com/Nurflugel/Northrop/northrop.html).
- [22] J. D. Anderson, Fundamentals of Aerodynamics, New York: McGraw-Hill, 2001.
- [23] J. Mizrahi, „Flight of the future,“ April 1999. [Online]. Available: <http://www.twitt.org/bldwing.htm>.
- [24] Grote und Feldhusen, Dubbel, Aachen: Springer, 2007.
- [25] M. Badrocke, „Sobchak Security,“ 2005. [Online]. Available: <http://sobchak.wordpress.com/2009/08/26/cutaway-hawker-siddeley-avro-vulcan-b-mk-2/>.
- [26] E. Torenbeek, Advanced Aircraft Design: Conceptual Design, Technology and Optimization of Subsonic Civil Airplanes, Delft: Wiley, 2013.
- [27] D. Scholz, „Presentation for EWADE, Student Project of a Blended Wing Body,“ 2007. [Online]. Available: [http://www.mp.haw-hamburg.de/pers/Scholz/ewade/2007/EWADE2007\\_Scholz.pdf](http://www.mp.haw-hamburg.de/pers/Scholz/ewade/2007/EWADE2007_Scholz.pdf).
- [28] „Operating the 747-8 at Existing Airports,“ The Boeing Company, 2010. [Online]. Available: [www.boeing.com/commercial/aeromagazine/articles/2010\\_q3/3/](http://www.boeing.com/commercial/aeromagazine/articles/2010_q3/3/).
- [29] H. S. W. Gross, Technische Mechanik 2, Berlin: Springer, 2009.
- [30] ThePointsGuy.com, 2014. [Online]. Available: [http://thepointsguy.com/2012/10/maximizing-the-newest-business-and-first-class-products-on-us-airlines/img\\_business\\_class\\_seats/](http://thepointsguy.com/2012/10/maximizing-the-newest-business-and-first-class-products-on-us-airlines/img_business_class_seats/).
- [31] Landau und Lifschitz, Lehrbuch der theoretischen Physik - Hydrodynamik, Moskau: Harri Deutsch, 1984.
- [32] J. Katz und A. Plotkin, Low-Speed Aerodynamics, Cambridge University Press, 2001.
- [33] Schlichting und Truckenbrodt, Aerodynamik des Flugzeuges, Erster Band, Göttingen: Springer, 1967.
- [34] L. Prandtl und A. Betz, Vier Abhandlungen zur Hydrodynamik und Aerodynamik, Göttingen: Selbstverlag des Kaiser Wilhelm Instituts für Strömungsforschung, 1927.
- [35] Zhang, Rizzi, Nangia, Amiree und Amoignon, „Aerodynamic Design Considerations and Shape Optimization of Flying Wings in Transonic Flight,“ *12th AIAA Aviation Technology, Integration and Operations (ATIO) Conference and 14th AIAA/ISSM, Indianapolis, Indiana*, September 2012.
- [36] NASA, „Aviation Pioneer Richard T. Whitcomb,“ 2009. [Online]. Available: [www.nasa.gov/topics/people/features/richard\\_whitcomb.html](http://www.nasa.gov/topics/people/features/richard_whitcomb.html).